2012

Dissecting Synaptic Vesicle Endocytosis

Moritz Armbruster

Dissecting Synaptic Vesicle Endocytosis

A Thesis Presented to the Faculty of

The Rockefeller University

in Partial Fulfillment of the Requirements for

the degree of Doctor of Philosophy

by

Moritz Armbruster

June 2012

DISSECTING SYNAPTIC VESICLE ENDOCYTOSIS

Moritz Armbruster, Ph.D.

The Rockefeller University 2012

Synaptic vesicle endocytosis is critical for ensuring rapid local recycling of synaptic vesicles to enable ongoing neuronal activity. We utilized the sensitivity and robustness of the pHluorin assay of synaptic vesicle recycling to probe the control of endocytosis spatially and in response to varying stimulation conditions. We examined the role of the large GTPases dynamin 1 and dynamin 3 in synaptic vesicle endocytosis; which have been thought to be essential for the fission of budding vesicles from the plasma membrane. Dynamin 1, 3 and 1/3 double knockouts indicated that there is redundant presynaptic function of the proteins. Loss of either protein alone results in a subtle phenotype; only in the double knockout is synaptic vesicle endocytosis strongly impaired. However, even lacking both dynamin 1 and dynamin 3 synaptic vesicles can still undergo many rounds of exocytosis and endocytosis.

Individual nerve terminals from the same neuron often differ in neurotransmitter release characteristics. The extent to which endocytic retrieval of synaptic vesicle components differs across nerve terminals from the same axon is unknown. We used pHluorin-based assays to undertake a large-scale analysis of endocytosis kinetics of individual boutons. Our data indicates that endocytosis kinetics are primarily set at a cell-wide level rather than at that of individual boutons. We observed a $\sim$4 fold range in cell wide time constants (from 5s to 20s) that was not dependent upon the type of neurotransmitter being utilized (excitatory/inhibitory), nor the history of activity of the neuron.

In addition to cell to cell variation in endocytic kinetics, we also explored the modulation of endocytosis by the stimulation and/or Ca^{2+} influx. We demonstrated two regimes of Ca^{2+} modulation, a Ca^{2+} dependent acceleration for small stimuli and a Ca^{2+} dependent slowing for larger stimuli. The acceleration is especially prominent at physiological temperature, accelerating the endocytic time constant by 50% over 25AP at 10Hz. The acceleration has a persistence time >20s suggesting an optimization of endocytosis for infrequent bursts of activity. Utilizing the dynamin 1/3 double knockout we showed that the acceleration depends on the successful dephosphorylation of dynamin at 2 serines previously identified as substrates for the Ca^{2+} dependent phosphatase, calcineurin. Removal of the F-Bar domain protein syndapin 1, a dynamin 1 binding partner that requires dynamin 1s dephosphorylation, also distortedthe acceleration.

We examined the setpoint of synaptic vesicle endocytosis between boutons, between cells, and under different stimuli conditions; indicating that there is a lot of potential for modulation of the endocytic kinetics: a 4 fold range of cell wide modulation and a stimulus dependence that shows evidence for a clear optimal stimulus for minimizing the endocytosis time constant in a dynamin phosphorylation state dependent manner.

Acknowledgements

I would like to thank Tim Ryan, for the great experience I had in the lab. He has provided enthusiasm, mentorship and support which have not only made this study possible, but also an enjoyable learning experience. Likewise I would like to thank all the members of the lab, for the countless advice and help: Balaji, Pablo Ariel, Sung Hyun Kim, Meera Mani, Ricky Kwan, Ping-Yue Pan, Vidhya Rangaraju, Mike Hoppa, and Yogesh Gera. They have taught me many things and have become my friends. I would like to especially mention, Balaji, whose work I followed up both scientifically and in tinkering with the microscopes. In our brief overlap and in his handiwork he has taught me many things on dealing with the microscopes. Secondly, I would like to mention Ricky Kwan and Yogesh Gera, who provided excellent technical assistance with the cultures and transfections. I would like to thank Sung Hyun Kim for expert advice regarding all things molecular biology, all things related to Calcineurin and AP-2. Mike Hoppa and Pablo Ariel were always available to bounce ideas off of, and made the lab a lot more exciting of a lab. I would also like to mention Jeremy Dittman, whose suggestions, advice, and conversations have been very stimulating and insightful. My brother Benjamin has always been a great source for statistical advice and someone to probe with random questions.

I would like to thank Pietro De Camilli, Shawn Ferguson, Mirko Messa, and others at Yale who created the dynamin knockout mice, generously provided them along with plasmids for our use and with whom we have collaborated on these projects. They have been very supportive, with good discussions.

I would like to thank my committee members David Gadsby and Marcelo Magnasco for their support, and advice at our yearly meetings.

I would also acknowledge the support of the Dean's office at Rockefeller University and the support staff in the Cornell Biochemeistry Department who have isolated me

from many hassles and have generally made everything function very smoothly.

I would like to thank my parents Charlotte and Dieter for their support. And my friends Manuel and Matt without whom it would be a lot less interesting of a place. Last but not least Anne and Sputnik for making this last year exciting, and adventurous.

Table of Contents

List of Figures

1. Introduction

How synaptic strength is determined is an important question in neuroscience. Several different aspects of synaptic biology can affect synaptic efficacy: post-synaptic receptor trafficking, pre-synaptic exocytosis properties, pre-synaptic vesicle availability and many others. The mechanisms of how synaptic vesicles are recycled and made release competent after exocytosis has been a crucial question for several decades. Small central synapses contain only 100 vesicles per pre-synaptic terminal [9, 34, 85, 86], of those only half or fewer appear to participate in synaptic transmission as part of the recycling vesicle pool. Thus there are very few release competent vesicles per terminal, making efficient recycling of these vesicles critical to supplying the exocytic pathway. Determining the time scale and mechanism of this process has been of interest in the field for a long time. One of the earliest observations of synaptic vesicle cycling in action was by electron microscopy (EM) carried out in classic studies by John Heuser. Rapid freezing followed by EM was used to conclusively demonstrate that exocytic fusion pores could be captured at active zones when the specimen was frozen a few milliseconds after the stimulus. In the same experiments invaginations corresponding to endocytic pits were observed over a much longer time scale 30s after the stimulation [62] at locations peripheral to the active zone. In the last 15 years this process has been probed using EM, fluorescent lipophillic dyes, capacitance measurements, and genetically encoded probes. All of these have helped refine our understanding of the mechanism, kinetics and proteins involved in synaptic vesicle endocytosis.

1.1 Endocytosis Kinetics

One of the fundamental questions in the field has been what controls and/or modulates the kinetics of endocytosis and the relevance of these controls to physiological function. Synaptic vesicle endocytosis shares many components with canonical clathrin-mediated endocytosis in non-neuronal cells; however, it is a very specialized form. Even different neuronal systems show different endocytosis kinetics; measurements in the goldfish Bipolar cells or at the Calyx of Held have shown mono or bi-exponential vesicle recoveries depending upon the intensity of the stimulation [67,107]. This was seen both for step depolarizations and trains of action potential equivalent stimulation. Additionally, loading synapses with the Ca^{2+} chelator EGTA prevented the appearance of a bi-exponential phase. In small central synapses endocytosis has a single kinetic phase, following a single exponential recovery [9,30]. Single vesicle endocytosis has been shown to follow an exponential random distribution; which when extrapolated for the ensemble case agrees very well with the observed kinetics [9]. Based upon the single exponential decay, these results suggested that there is a single rate limiting step in the endocytic process. These results underlie the basic assumptions of our models of the endocytosis time constant in chapter 4. In midbrain dopaminergic neurons endocytosis has been shown to be considerably slower than in hippocampal cultures [60]; indicating that there is some brain region specificity to the process. Many previous observations were done at room temperature and the evidence indicates that endocytosis accelerates considerably at physiological temperature [8,61,74]. Additionally, it is known that the action potential narrows with increasing temperature [37], which in turn will limit calcium entry. These features raise questions about what the physiologically relevant Ca^{2+} dependent mechanisms for modulating endocytosis are. Two of the know ways to change endocytosis kinetics is changes in the endocytic load and changes in Ca^{2+} influx. The endocytic load, defined as the number

of vesicles to be endocytosed after a given stimulus, is tightly linked with the number of vesicles exocytosed, which is also a highly Ca^{2+} sensitive process. Therefore deconvolving the Ca^{2+} dependence of release and the Ca^{2+}/load effects on endocytosis has been difficult. Endocytosis in Goldfish Retinal Bipolar cells is inhibited by high levels of intracellular Ca^{2+}: rapid elevations in intracellular calcium led to dramatic slowing of endocyticis. This effect was largely independent of the amount exocytosed and the Ca^{2+} dependence could be described with a Hill equation with a cooperativity of 4 and $K_{1/2}$ of 460nM [104]. In mouse inner hair cells, photolysis of caged Ca^{2+}, specifically triggered a fast mode of endocytosis. This effect was prevalent above 15μM uncaged Ca^{2+} and retrieves a significant amount of membrane in <1s [11]. Measurements in the the Calyx of Held, a giant auditory brain stem synapse, showed that increasing Ca^{2+} influx slows the endocytosis time constant [94]. Studies in rat and mouse primary neurons in culture showed that endocytosis could be modulated by changing extracellular Ca^{2+} and/or stimulus frequency. Early studies showed that increasing the stimulus number prolonged endocytosis [82] while an examination over smaller stimuli showed that endocytosis is invariant [8, 31]. Lowering extracellular Ca^{2+} generally slowed endocytosis in this system [84,108]. These results demonstrate contradictory modulations for overlapping stimulus, load, and Ca^{2+} regimes; and it is not clear what the relevant behavior is for physiological stimuli. Two reported effects, Ca^{2+} inhibition of endocytosis and that Ca^{2+} stimulation of endocytosis are seen; however, the balance between the two effects is unclear. Potential Ca^{2+} sensors for endocytosis have been identified, synaptotagmin [70, 112], calcineurin [46, 53, 95], and calmodulin [95, 113]. Genetic ablation of synaptotagmin 1 shows severe defects in presynaptic exocytosis and endocytosis; which can be rescued independently with different domains/mutations of synaptotagmin 1 [70, 112]. This defect is not present when exocytosis is triggered by hypertonic sucrose which is thought to function in a Ca^{2+} independent manner. While essential, synaptotagmin 1's Ca^{2+} sensitivity is not

linked to the Ca^{2+} dependent slowing or acceleration of endocytosis. Calcineurin is another candidate for an endocytic calcium sensor, pharmacological inhibition shows defects in endocytosis [54,55,58]. Calcineurin is the phosphatase for the dephosphins, synaptic proteins that are dephosphorylated by activity [58]. Many of the dephosphin proteins: dynamin, amphiphysin and synaptojanin, are involved in endocytosis. The role of changes in the phosphorylation state of these proteins however remains unclear. Calcineurin also determines the size of the recycling pool and modulates the Ca^{2+} influx [46, 47]; therefore extracting calcineurins endocytic contributions rather than secondary effects has been difficult. Experiments using pharmacological inhibition of calmodulin indicate that this calcium binding protein is essential for initiating endocytosis [95, 108] however experiments at the Calyx of Held indicated that calmodulin only engages for very strong stimuli, and rates of endocytosis for smaller stimuli were not affected [113]. Although these different calcium binding proteins all appear to function in endocytosis the link between specific Ca^{2+} dependent endocytic behaviors and a the role of one of these Ca^{2+} sensors has not been established. As a result it is not clear if these Ca^{2+} sensors are relevant for physiological stimuli. In addition to probing the physiological modulation of endocytosis a number of studies also used genetic and pharmacological perturbations to identify the control mechanisms. Many different perturbations that make use of ablation of expression of different proteins result in slowing the time constant of endocytosis. One particular perturbation however additionally changes the kinetic profile. Genetic ablation of expression of the clathrin adaptor protein AP-2 in hippocampal neurons changes vesicle recovery kinetics from a single exponential to a bi-exponential process with one time constant faster than the wild type single exponential time constant and one slower [45]. This suggests that multiple pathways that are repressed under normal conditions might be compensating the lack of AP-2. Most other modulations affect the time constant of the exponential recovery or introduce a baseline offset rather than the shape of the

recovery. Proteins shown to affect the endocytosis time constant include, synaptojanin [59], dynamin 1 [25], endophillin [28,63], and auxilin [114]. Some show a drastic slowing of endocytosis including clathrin [30]. Although numerous other proteins have been implicated in synaptic vesicle endocytosis often the techniques used to examine the consequence of their ablation dont provide a direct readout of the endocytosis kinetics. This includes amphiphysin [22, 24], epsin [43], syndapin [1, 50]. In general one common theme that has arisen from genetic perturbations is that endocytic process is very robust: most perturbations induce small endocytic defects. Some of this robustness might arise from the presence of multiple isoforms such as mammalian dynamin (3 genes), syndapin (3 genes), or endophilin (3 genes); additionally it is possible that other trafficking proteins may compensate for their absence.

1.2 Synaptic vesicle identity

Under what conditions do vesicles retain their identity? Two distinct theories address this question from a variety of approaches. Kiss and Run as an endocytic mechanism proposes that a vesicles identity is maintained through several rounds of fusion and closure of the fusion pore. Full collapse and fusion proposes vesicle proteins diffuse on the plasma membrane and get reincorporated into newly formed vesicles. All of these theories approach the fundamental question of how are vesicles reliably recycled while maintaining the precise stoichiometry of vesicle proteins as found in the synaptic vesicle proteome [97]. Does endocytosis prefer recently exocytosed vesicle components over the membrane resident fraction? Klingauf and colleagues have provided evidence for a readily endocytosible pool whereby upon fusion some vesicular proteins are specifically excluded from the newly formed vesicle and instead copies of these proteins already resident on the plasma membrane are preferentially endocytosed [41, 105]. pHluorin-tagging of synaptic vesicle proteins allows one to determine

what fraction of these are resident on the plasma membrane at any given time [82]. Selective photobleaching experiments showed that large stimuli result in even mixing between exocytosed components and surface resident components when generating new endocytic vesicles as a proportional fraction of both are endocytosed [26,41,105]. Wienisch and Klingauf however showed that for small stimuli (<40AP) there is a preference for internalizing components from the surface fraction. This led to the theory of a readily retrievable pool of presorted vesicles components on the membrane surface that would be endocytosed as soon as a vesicle was released. This suggests that for small enough stimuli there should be a kinetic advantage because the need to sort the vesicle components is alleviated [41]. However, for small stimuli it is difficult to distinguish between the readily retrievable pool and mixing with the surface pool, and the matter remains unsettled.

The complexity of the process of regathering and sorting of synaptic vesicle protein components on the plasma membrane have bolstered the appeal of a process like kiss and run which would maintain vesicle identity and bypass this problem. In Kiss and run it is proposed that vesicles transiently open a fusion pore, release some amount of neurotransmitter, and then the fusion pore reseals. This theory implies that subquantal transmission is possible, and that vesicles can fuse repeatedly many times. The appearance of transient fusion pores has been observed by capacitance measurements directly in large dense core vesicles of neuroendocrine cells [49,79,117] as well as in the the Calyx of Held [106]. In the Calyx of Held it is not the dominant mechanism of vesicle recycling and there are some criticism that these observations could be due to artifacts [91]. In small central synapses direct observation of these transient fusion events have been difficult and the evidence for kiss and run has been based on indirect measurements. Early measurements were based upon sub-quantal destaining of the lipophillic dye FM1-43 [71], modulation of FM1-43 fluorescence by an extracellular quencher [4], and pH sensitivity of quantum-dot-bearing synaptic

vesicles [115, 116]. In general these studies have relied on identifying fast endocytic events as a signature of kiss-and-run. However measurements of the endocytosis times for single vesicles indicated an exponential distribution of endocytosis time constants and thus predict that some events will always be fast [9].The full collapse and fusion mechanism could explain very fast events and on average provide sufficiently fast endocytosis to maintain exocytosis [8].

Another approach to dissecting these two possible endocytic pathways has been to genetically or pharmacologically inhibit proteins involved in one of the endocytic mechanism specifically. The full collapse and fusion is thought to require the endocytic machinery involving clathrin dependent endocytosis. Knocking down clathrin with a shRNA construct showed that the vast majority of synaptic vesicle endocytosis is clathrin dependent [31]. Similarly, as mentioned previously perturbations of many of the classic proteins involved in clathrin mediated endocytosis have been shown to slow synaptic vesicle kinetics. Meanwhile there has been a lack of molecular components specific for kiss and run endocytosis. Throughout this controversy the evidence if kiss and run occurs in these synapses is mixed, but suggest that full collapse and fusion is the primary mechanism for synaptic vesicle endocytosis in hippocampal synapses. If kiss and run occurs it does not play a significant role in determining the synaptic vesicle endocytosis kinetics and is not observable using the pHluorin assay of synaptic vesicle endocytosis.

1.3 Endosomes and Bulk Endocytosis

Early EM images of presynaptic terminals indicate the presence of large endosome like membrane compartments [35]. These structures have been proposed to play a roles in the sorting step for synaptic vesicle components [69] and/or as a result of a bulk endocytic pathway which can internalize large pieces of membrane under high endo-

cytic load. EM shows that the endosome like structures are very transient, occurring between 4-30s after stimulus and they appear in a stimulus dependent manner [35,98]. Molecular components required for endosomal fusion are present in newly endocytosed vesicles [39, 76]; suggesting that these structures could serve as a sorting step. The pathway has been labeled with lipophillic dyes, FM1-43/FM2-10, or with fluorescent dextran particles [16,38,75,99]. Small central synapses show labeling after 80Hz stimulation for 10s, while lower frequency stimulation fails to trigger this mechanism [19]. In the Calyx of Held, capacitance measurements indicate internalization of 1-3um structures, which was attributed to a bulk endocytic pathway. These events occurred infrequently, but their occurrence was also modulated by the intensity/duration of the depolarization [106]. The only molecular perturbation affecting the bulk endocytosis assays is the phosphorylation state of dynamin [3, 17, 20, 110]. The stimulation required to desphosphorylate a significant fraction of the dynamin is similar to the large stimuli that trigger bulk endocytosis [18]. The studies have shown the existence of these endosome like structures and possible large membrane internalizations; however, it remains unclear if they contribute to synaptic vesicle formation. The stimuli inducing these internalization are extremely large where their physiological relevance is unclear. The outstanding question in the field is how/where the synaptic vesicle components are sorted and the possible involvement of the endosome like structures.

1.4 Dynamin

Mutant alleles of dynamin were first isolated in a screen for temperature sensitive paralytics in drosophila. One of the most prominent mutants was the shibire mutant which showed dramatic block of endocytosis, revealed as a dramatic loss of synaptic vesicles when synapses were stimulated at elevated temperatures [52]. Dynamin was also purified originally as a brain microtubule binding protein and named because

of a suspected motor activity [87]. Sequencing of the dynamin gene showed that it was the same as the shibire gene [15, 102]. The protein dynamin was originally identified as a dephosphin, a synaptic protein that undergoes dephosphorylation upon activity [77]. Dynamin is a large GTPase, and is thought to function in the process of fissioning a budding vesicle from the plasma membrane. Mice contain three dynamin genes; DNM1 the dominant brain isoform, DMN2 ubiquitously expressed, but present at very low levels in the brain, and DNM3 specific to brain and testes, but at much lower levels than DNM1 [25]. Dynamin contains five domains: an N-terminal GTPase domain, a middle domain, a plexstrin homology (PH) domain, a GTPase effector domain (GED), and a proline rich domain (PRD). The middle domain is involved in assembly of dynamin into higher order structures [73]. The PH domain interacts with phosphoinositides localizing dynamin to the plasma membrane and oligerimization [48]. The GED domain is a GTPase activating protein (GAP) [64]. The PRD domain interacts with SH3 domains of other endocytic proteins including endophilin, syndapin, and amphiphysin [2]. Seven phosphorylation sites have been identified [29] in the long spliceform of dynamin 1. Five undergo activity dependent dephosphorylation. The two dominant phosphorylation sites are in the phosphobox of the PRD at serine 774 and 778. These account for $\sim$70% of the P32 incorporated in the assay [29]. Understanding the significance of the phosphorylation state has been limited to biochemical assays showing phosphorylation state dependent binding in the PRD of the F-bar protein syndapin [2, 3]. Calcineurin, the Ca^{2+} dependent phosphatase, dephosphorylates dynamin and CDK5 and GSK3β rephosphorylate the phosphobox [20, 29, 58, 110]. Dynamin 1 has two splicing sites, one in the middle domain and one in the PRD [13]; however, no expression differences in the spliceforms are identified. A short spliceform of the PRD of dynamin 1 binds selectively to calcineurin; however, its functional significance has not been determined [110].

The dominant negative effects of shibire-ts in drosophila and non-hydrolysable

GTPγS at the Calyx of Held led to the conclusion that dynamin is indispensable for synaptic vesicle endocytosis [51,52,109,111]. In non-neuronal systems, overexpression of a dominant negative dynamin GTPase mutant strongly inhibits transferrin internalization [36,92]. In vitro experiments show that dynamin is sufficient to cause fission of liposomes, and wraps around the liposome in large spiral structures in the absence of GTP [78, 96]. It has also been shown that the presence of dynamin transiently stabilizes the restricted membrane, and only upon unbinding does the membrane collapse [10]; suggesting a direct role in inducing membrane fission. In the Calyx of Held, dynamins essential role has been inferred based upon patch loading of non-hydrolyzable GTP analogs, along with inhibitory peptides; both perturbations show an almost complete block of endocytosis [109,111]. Similarly, injection of SH3 domain peptides that should disrupt dynamins ability to bind other endocytic proteins, into the giant reticulospinal synapses in lamprey resulted in many stranded vesicles stuck on the plasma membrane, presumably unable to undergo fission [88]. Lastly, small molecule inhibitors have also been used to inhibit dynamin, which supports the view of dynamins essential role for endocytosis [33,68]. Remarkably however cortical neurons dissociated from dynamin 1 KO mice brains shows surprisingly subtle phenotypes. The dynamin 1 KO shows only an inhibition of endocytosis during the stimulation, as assayed by synapto-phluorin, and an abundance of activity dependent membrane bound clathrin coated pits by electron microscopy [25]. The post-stimulation endocytosis kinetics was unaffected by loss of dynamin 1. Based upon the subtle phenotype in the dynamin 1 KO we characterize the dynamin 1/3 double knockout (DKO), to further reduce the level of dynamin and probe its significance in small central synapses. These studies showed a much more dramatic phenotype which permitted for the first time a detailed structure-function analysis of dynamin in living synapses.

2. Materials and Methods

2.1 Cell culture and Imaging

Hippocampal CA3-CA1 regions were dissected from 1- to 3-d-old Sprague Dawley rats, dissociated, and plated onto poly-ornithine- coated glass for 1426 d as described previously [80]. For experiments utilizing the dynamin knockout mice and controls cortexes were dissected from postnatal 0 to 1 day old mice were dissociate and plated onto poly-ornithine coated glass as previously decribed [25]. Cultures were transfected with calcium phosphate 7-8 days after plating and imaging was performed 13-26 days after plating (5-18 days after transfection). The primary reporter used was a chimera of the pH sensitive GFP, pHluorin and the vesicular glutamate transporter made by Voglmaier lab. pHluorin has a pKa of 7.1, and undergoes a 20 fold increase in fluorescence with the pH shift of 5.5 in the vesicle lumen to 7.4 in the outside media [82]. From quantal analysis 1-2 copies of the pHluorin reporter is present per vesicle [9, 89]. To allow for retrospective staining of excitatory and inhibitory neurotransmitter transporters we used a chimera of pHluorin and synaptophysin as our reporter [118]. For Ca^{2+} imaging experiments Vamp2-mCherry fusion protein was used to mark the transfected cells after loading cells with Ca^{2+} dye Fluo5F-AM at 100μM for 10min [6]. For AP2 knockdown experiments a previously created knockdown construct was co-transfected with the reporter [45]. For knockdowns of synapdin 1 a shRNA knockdown construct was purchased from Origene (Rockville,

MD, USA) with the following sequence: GTATGCCACCGAGTGGTCAGACGATGAGA. Constructs for dynamin 1 long (bb) and short spliceform (ba), dynamin 2, dynamin 1 S774/8A, dynamin 1 S774/8D, and syndapin 1 rescues were provided by the De Camilli Lab (Yale University, New Haven, CT, USA) [25].

Coverslips were mounted in a rapid-switching, laminar-flow perfusion and stimulation chamber (volume $\sim 75 \mu l$) on the stage of a custom-built laser-illuminated epifluorescence microscope. Cells were perfused with a solution containing in mM: 119 NaCl, 2.5 KCl, 2 $CaCl_2$, 2 $MgCl_2$, 25 HEPES (buffered to pH 7.4), 30 glucose supplemented with 10 μM 6-cyano-7- nitroquinoxaline–2,3–dione (CNQX), and 50uM D,L-2-amino-5-phosphonovaleric acid (AP5). AP2-KD experiments were incubated with 1μM Brefeldin-A before imaging to ensure a single exponential decay [45]. Cells were treated with ammonium chloride solution (pH 7.4), by replacing 50mM saline with NH4Cl and acid quenchs (pH 5.5) by replacing HEPES with MES, to measure surface fraction [83] and surface availability. For experiments involving 4mM Ca^{2+} tyrodes solution, $CaCl_2$ was swapped for $MgCl_2$. All chemicals were obtained from Sigma. Due to the low surface fraction of vG-pH [9], we gave brief bursts with 6 APs at 30 Hz every 4 s to find transfected cells in a dish. Perfusion was kept between 75-250μL per minute to ensure prolonged cell survival. Cells were imaged either at room temperature Dynamin DKO chapter, 30°C Variability chapter, or 36.8°C Ca^{2+} dependence chapter by heating the microscope objective with a flexible resistive heater (Omega, CT,USA) utilizing either a proportional current controller (Minco, MN) with custom amplifier or a On-Off controller (Minco), which maintained the temperature at the objective within ± 0.1°C as readout by a 100Ω platinum thermistor (Minco). The coverslip was measured to be within 0.5°C of the objective temperature as measured with a thermocouple. Utilizing a 488nm (pHluorin, fluo5-F) and/or 561nm (vamp-mCherry) diode pumped solid state laser (Coherent, CA), shuttered using an acouto-optic modulation during all periods without data acquisition. Flu-

orescence excitation and collection was through a 40X 1.3 NA Fluar Zeiss objective using 515-560 nm emission and 510 nm dichroic filters (Chroma, VT) and a 1.6X Optivar tube lens. Laser power at the back aperture was ∼1 mW, imaging onto a Andor iXon+ (model number DU-897E-BV) back-illuminated electron-multiplying charge coupled device camera in epifluorescence. Action potentials were evoked by passing 1ms current pulses, yielding fields of ∼10V/cm via platinum-iridium electrodes from an Isolated current stimulator (World Precision Instruments, FL).

For immunostaining of knockdown levels (AP2, Syndapin I), and neurotransmitter type classification (vGlut, vGat) cells were fixed after the experiment with with 4% paraformaldehyde and permeabilized with 0.2% Triton X–100, blocked with 5% bovine serum albumin. Cells were subsequently stained with anti-green fluorescent protein (Invitrogen, CA), anti–α–adaptin (ABR, CO), anti-vGlut (Millipore,MA), anti-vGat (Millipore,MA), Syndapin I (Synaptic Systems, Goettingen, Germany) and utilizing secondary antibodies conjugated to Alexa Fluor 430, 488, 546, 633 (Invitrogen, CA). Immunofluorescence images of fixed cells were acquired using a custom built laser scanning microscope with custom-written control software. For cell type classification staining patterns were compared to untransfected cells within the same culture dish to classify cells as excitatory or inhibitory. For knockdown experiments, transfected cell bodies were compared to surrounding untransfected cell bodies, to characterize the level of knockdown.

2.2 Image and data analysis

Images were analyzed in ImageJ (http://rsb.info.nih.gov/ij/) using a custom-written plugin (http://rsb.info.nih.gov/ij/plugins/time- series.html). 2μm diameter circular ROIs were placed on all varicosities based upon the delta-F image of a 100AP 10Hz run. Only boutons that did not split or merge, remained in focus and responded

throughout all trials were chosen. All fitting was done using OriginPro (OriginLab, MA) with the Levenberg-Marquardt algorithim. Fits were single exponential decays with an offset for reacidification 2-3s as described previously [8]. In general, fits were conducted on the ensemble average of each run, or multiple runs for very small stimuli. For physiological Ca^{2+} dependence studies, each cell was normalized to its 100AP 10Hz behavior to avoid the cell to cell variations in time constant that we observed earlier. Surface fraction was calculated from NH4Cl traces as described earlier [82].

2.2.1 Single bouton fitting

Cells were imaged at 4 Hz for 200-300 frames, adjusted based upon the decay time of the first run. Cells were imaged until cell morphology or kinetic changes indicated the onset of cell-rundown to maximize the number of the runs acquired. It was found that allowing 5 min spacing between stimulations allows for the largest numbers of runs to be acquired. Rundown was judged based upon the average endocytic time constant for each run. The inclusion criteria were: a signal to noise ratio of at least 10 for the exocytic response over the baseline fluctuation; the normalized chi-squared value of the single exponential had to be less than 5; runs whose predicted time constant was within a measurable range given our imaging conditions; a minimum of 5 fittable runs were required to include an individual bouton in the analysis. Upon visual inspection, no included fit could be excluded on qualitative grounds; additionally, there was no systematic exclusion of good fits or reason beyond the quality of the signal for exclusion of bouton-events. On average 61% of the bouton-events passed our fitting criteria. When examining variations in the cell average time constants (Fig 4.7b), in a subset of cells (55/84) the cell average time constant was calculated by fitting each cell averaged run. The average standard error for these cell average time constants is 0.9s.

2.3 Simulations

2.3.1 Endocytosis during stimulation

Previous work showed that endocytosis is a continuous function during and after stimulus [8]. To verify if this continuity is maintained in the dynamin knockouts we developed a simple model of endocytosis during stimulation based upon the measured post-stimulus dynamics of endocytosis. Assuming the dynamics of endocytosis after stimulation are a good approximation for the dynamics during stimulation base upon previous studies [8, 25]; a system of first order differential equations was setup to model the exocytosis-endocytosis-reacidification steps. Exocytosis is approximated as a constant rate of release, the value of which was measured from bafilomycin traces. The time constants for endocytosis are assumed based upon the post-stimulus endocytosis. The reacidifcation parameter is assumed from previous work measuring the rate [7, 30].

Figure 2.1: First order model of synaptic vesicle cycle

Constant rate of exocytosis ∼80% of the pool exocytosed in 30s measured from the bafilomycin rise. Exocytosis rates as percentage of the pool were similar in knockout versus wild-type. Endocytosis time constants are converted from $t_{1/2}$ times in figure 3.1, for WT, Dynamin 1 KO, and Dynamin 3 KO. The decays are well described by single exponential decays, while for the dynamin 1/3 DKO the rate of decay is too slow to determine if it follows an exponential decay, which could be a source of error.

Time constant for reacidification = 4s

Time constant for WT endocytosis = 24.5s

Time constant for Dynamin 1 KO endocytosis = 33.0s

Time constant for Dynamin 3 KO endocytosis = 21.9s

Time constant for Dynamin 1/3 DKO endocytosis = 118.7s

System of two first order differential equations:

$$\frac{d}{dt}surface(t) = k_{exo} - k_{endo}surface(t) \tag{2.1}$$

$$\frac{d}{dt}alkaline(t) = k_{endo}surface(t) - k_{acid}alkaline(t) \tag{2.2}$$

$$surface(0) = 0 \tag{2.3}$$

$$alkaline(0) = 0 \tag{2.4}$$

$$Fluorescence(t) = surface(t) + alkaline(t) \tag{2.5}$$

$$Fluorescence(t) = \frac{k_{exo}(k_{endo} - k_{endo}e^{-k_{acid}t} - k_{acid}e^{-k_{endo}t})}{k_{acid}(k_{acid} - k_{endo})} - \frac{k_{exo}(-1 + e^{-k_{endo}t})}{k_{endo}} \tag{2.6}$$

2.3.2 Vesicle Estimate

To estimate the number of vesicles released we measure the fraction of the recycling pool released, $24 \pm 4\%$ (n=8 cells). Based upon a previous result which measured the quantal fluorescence from a single vesicle and measured the average recycling pool size in similar cultures to be 64 ± 14 vesicles [9]. This allows us to estimate the number of vesicles release for a 100AP 10Hz stimulus.

2.3.3 Markov Model

To model the endocytosis time of several synaptic vesicles internalizing at a single synapse we begin with the previous model of stochastic reuptake of a single vesicle [9]. We assume that the endocytosis of any individual vesicle is governed by an exponential random variable X_i with parameter λ. Based upon previous findings, we assume that all vesicles endocytose independently and in parallel [8]. To model several vesicles

internalizing at a synapse we assume n vesicles present on the membrane surface awaiting internalization. We define the time until there are $n-1$ vesicles on the membrane surface as the random variable T_n. T_n is the time until the first of n vesicles with exponential endocytosis distributions X_i internalizes. Therefore it is the minimum of n identical exponential distributions with parameter λ, equivalent to an exponential distribution with parameter $n\lambda$. For computational simplicity we are modeling the reacidification as an instantaneous transition. This should not affect variations predicted based upon this model as each reacidification step is thought to be a bulk process, and not expected to yield stochastic variations.

$$X_i = exp(\lambda) \tag{2.7}$$

$$T_n = min(X_1, X_2, \ldots, X_n) = exp(n\lambda) \tag{2.8}$$

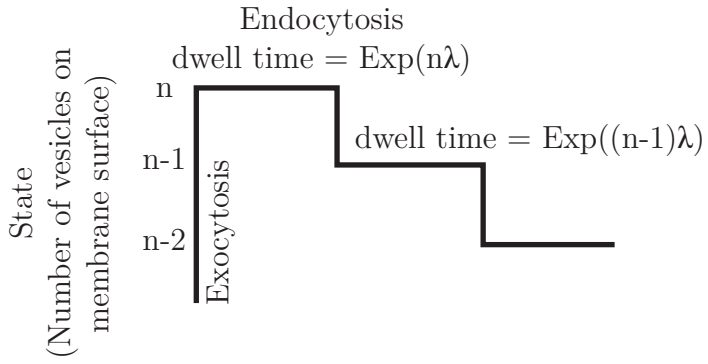

Figure 2.2: Markov model of expected endocytosis variations

This illustrates the transitions in the Markov model, from n to $(n-1)$ vesicles remaining to be endocytosed. To account for the time for all vesicles to endocytose we simply integrate the random variables for each transition step T_n from n to 1.

We need to account for the fact that the time constant of the fluorescence decay, measures the time until the fluorescence has decayed to $1/e$ of the initial. We can therefore define the random variable t_n as the endocytosis time constant at a given

synapse for and internalization of n vesicles.

$$\tau_n = \int_{\frac{n}{e}}^{n} T_i di \tag{2.9}$$

We can therefore calculate the expectation and variance of t_n

$$E = \frac{1}{\lambda} \int_{\frac{n}{e}}^{n} \frac{1}{i} di = \frac{1}{\lambda} \tag{2.10}$$

$$Var = \frac{1}{\lambda^2} \int_{\frac{n}{e}}^{n} \frac{1}{i^2} di = \frac{1}{\lambda^2} \left[\frac{e-1}{n} \right] \tag{2.11}$$

Additionally, we can solve for the number of vesicles released as a function of the coefficient of variation, CV, of the distribution. The observed CV and number of vesicles released in our data follow this relationship.

$$n = \frac{e-1}{CV^2} \tag{2.12}$$

While the expectation and variance of our model correspond well to our experimental data we want to compare the entire distribution of endocytic time constants. To easily generate a probability density function of this model we create a discrete approximation for the number of vesicles between n and n/e. Using this approximation, a probability density function of this Markov model can be generated based upon a Markov matrix of the model. The pdf can be fit with a maximum likelihood fit to the histogram of bouton events. The fits correspond well with the predicted expectation and variance (Fig. 4.4).

$$pdf(\tau_n(z)) = [1, 0, \ldots, 0] e^{z[\theta]} [\theta] \begin{bmatrix} 1 \\ \vdots \\ 1 \end{bmatrix} \tag{2.13}$$

$$\theta = \begin{bmatrix} -n\lambda & n\lambda & 0 & \dots & 0 \\ 0 & -(n-1)\lambda & (n-1)\lambda & & \vdots \\ \vdots & & \ddots & \ddots & 0 \\ & & & -(\lceil \frac{n}{e} \rceil + 1)\lambda & (\lceil \frac{n}{e} \rceil + 1)\lambda \\ 0 & \dots & & 0 & \lceil \frac{n}{e} \rceil \lambda \end{bmatrix} \tag{2.14}$$

2.3.4 Numerical Simulation

A numerical simulation of the model using a random number generator for each T_n internalization can incorporate variations in exocytosis between runs and boutons to estimate their contributions. The number of runs (25) in the simulated experiment is similar to the number of runs in our data set. We estimate the run to run variations in exocytosis based upon the CV of the pHluorin exocytosis step, ∼50% and use that to adjust the number of vesicles internalizing per bouton event. This simulation then predicts a CV between boutons of ∼12%, leaving an ∼13% CV remaining which could be due to biological variations between boutons.

3. Role of Dynamin in Synaptic Vesicle Endocytosis

3.1 Dynamin 1/3 Double Knockout

Dynamin is a large GTPase and mechanoenzyme that is thought to function in the fission step of endocytosis. There are three genes encoding mammalian dynamins, DNM1, DNM2, and DNM3. Dynamin 1 is the primary neuronal isoform, dynamin 2 is expressed ubiquitously, but at very low levels in neurons, and dynamin 3 is primarily neuronal, but at much lower levels than dynamin 1 [25]. Previous studies found very subtle defects in dynamin 1 KO mice, specifically the neurons were defective in endocytosis during prolonged stimuli [25] but showed relatively normal endocytosis kinetics immediately following the stimulus period. To investigate if the presence of dynamin 3 was masking a larger phenotype in the dynamin 1 KO mice, we performed measurements of recycling parameters in wild type, dynamin 1 KO, dynamin 3 KO and dynamin 1/3 double KO (DKO) neurons (Fig. 4). Both dynamin 1 KO and DKO neurons had much higher baseline vGlut1-pHluorin fluorescence than either the wild type or the dynamin 3 KO neurons, which were indistinguishable from one another Fig. 3.1a). NH4Cl and acid-surface quenching demonstrated that this difference was due to a much higher fraction of the reporter vGlut1-pHluorin being present on the plasma membrane, consistent with a steady-state impairment of endocytic function.

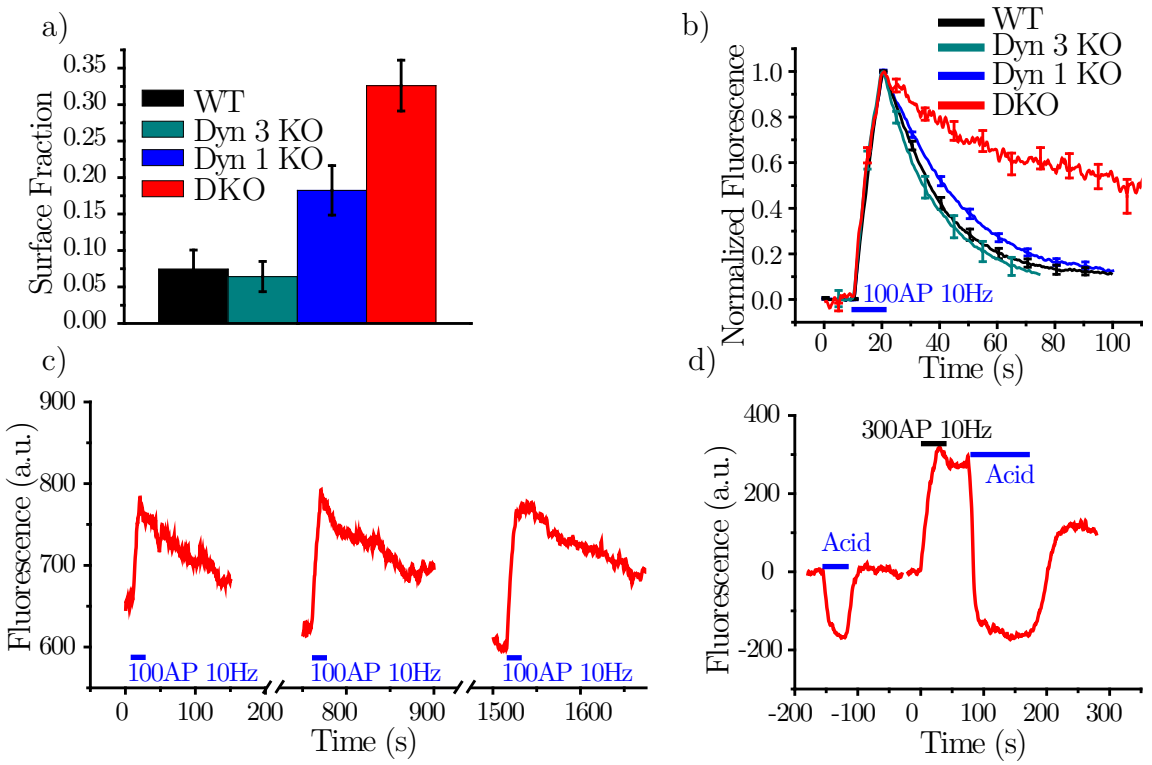

Figure 3.1: a)DKO and Dyn 1 KO cells have a greater fraction of the vGlut-pHluorin stranded on the surface. WT 7.4±2.6%, Dyn 3 KO 6.4±2.1%, Dyn 1 KO 18.3±3.4%, and Dyn 1/3 DKO 32.6 ± 3.5%. WT $n = 11$, Dyn 3 KO $n = 6$, Dyn 1 KO $n = 10$, and Dyn 1/3 DKO $n = 12$ cells. WT vs. Dyn 1 KO significant difference $p = 0.02$, Dyn 3 KO vs. Dyn 1/3 DKO significant difference with $p = 0.001$, Dyn 1/3 DKO vs Dyn 1 KO significant difference with $p = 0.008$, two sample t-test. b) Average vGlut-pHluorin traces. Endocytosis $t_{1/2}$ times WT 16.9±1.1s, Dyn 3 KO 15.1±3.1s, Dyn 1 KO 22.9 ± 1.7s, Dyn 1/3 DKO 82.3 ± 20.4s. Averaged from WT 40 runs 11 cells, Dyn 3 KO 22 runs 6 cells, Dyn 1 KO 43 runs 11 cells, Dyn 1,3 DKO 33 runs, 11 cells, see methods for error calculation. The difference in amount unendocytosed 40s after the end of the stimulus between WT and Dyn 1 KO is significant with $p = 0.02$, difference between Dyn 3 KO and DKO is significant with $p = 0.001$, two sample t-test. c) vGlut-pHluorin example trace of three consecutive runs from a dynamin 1/3 DKO cell showing responses to 100AP 10Hz stimulus,10 minutes between stimuli, 28 ROIs. $t_{1/2}$ times 62s, 90s, $> 140s$ d) Example trace of 300AP 10Hz response, with a pH 5.5 acid quench, showing that the fluorescence is quenched to an equivalent level to an unstimulated run with an acid quench.

Using the pHluorin assay, following the fluorescence increase evoked by a 100AP 10Hz stimulation, all 4 genotypes (Fig.3.1b) returned to baseline. Dynamin 3 KO mice have no apparent phenotype, and consistent wit this we found that endocytosis kinetics were unaffected by loss of dynamin 3. The pHluorin assays used here, based on tagging of vGlut1, are much more sensitive than those used originally to examine the Dynamin 1 KO. We therefore reexamined dynamin 1 KO with vGlut-pHluorin. Our analysis showed that synapses from dynamin 1 KO mice have a a small but statistically significant defect in endocytosis. However, the DKO showed much more severe impairment of the endocytosis kinetics. (Fig. 3.1b). The $t_{1/2}$ recovery times following 100 AP at 10 Hz stimuli were 16.9±1.1 seconds for wildtype, 15.±3.1 seconds for the dynamin 3 KO, 22.9±1.7 seconds for the dynamin 1 KO and 82.3±20.4 seconds for the DKOs, respectively, see Methods. Importantly, given sufficient time, the signal did recover in DKO neurons and their synapses could sustain multiple rounds of exocytosis and endocytosis (Fig. 3.1c). Multiple stimulations of the same neuron also revealed that while defective, endocytosis can still progress at a much slower rate. These slow recoveries were not simply a reflection of a slow re- acidification step, as the fluorescence during the recovery period could be fully quenched by perfusion with a solution of pH 5.5 (Fig. 3.1d) indicating that slow decay of vGlut-pHluorin signal arose from surface resident copies of this probe. Finally, a bafilomycin-based strategy that allows for separation of exocytic and endocytic contributions to the fluorescence traces [84] demonstrated a complete lack of endocytosis during the 10 Hz stimulus train at DKO synapses, as was previously observed [25], and now reconfirmed, at dynamin 1 KO synapses. In contrast, the loss of dynamin 3 alone had no effect (Fig. 3.2). However, unlike with the dynamin 1 KO, the absence of endocytosis during a 30 s stimulus period can in this case be attributed to the very slow post-stimulus kinetics see Methods.

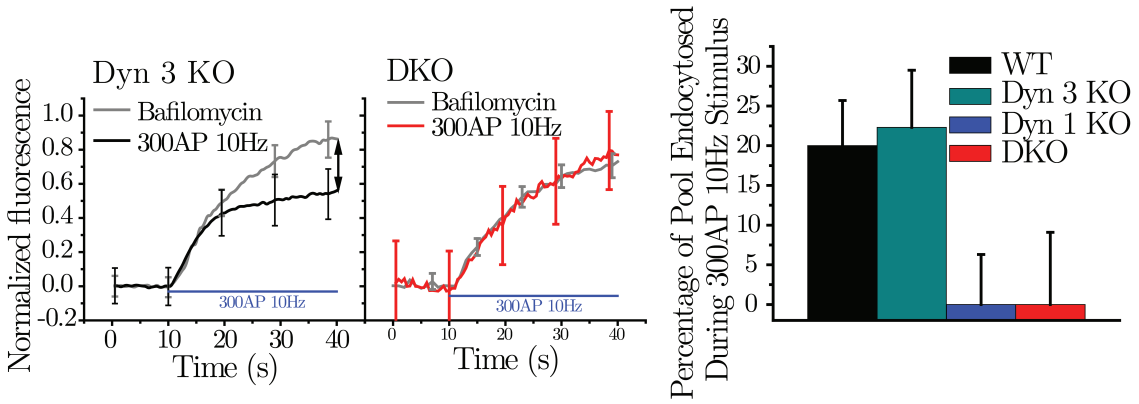

Figure 3.2: Endocytosis occurring during stimulation was measured by the difference between a 300AP 10Hz train and after full recovery, a subsequent 10Hz train in the presence of the proton pump inhibitor Bafilomycin. Runs are normalized to the maximum fluorescence obtained during stimulation in the presence of bafilomycin that represents the size of the recycling pool. Example traces from a Dyn 3 KO cell and a Dyn 1,3 DKO cell endocytosing 32.0% and 0% respectively. Averages are WT $20.0 \pm 5.7\%$ Dyn 3 KO $24.6 \pm 4.8\%$, Dyn 1 KO $0 \pm 6.3\%$, and Dyn 1,3 DKO $0 \pm 9.9\%$, from n=8, 5, 7, and 6 cells respectively. Difference between WT and Dyn 1 KO is significant with p=0.006, Dyn 3 KO and Dyn 1/3 DKO is significant with p=0.03, two sample t-test.

3.2 Discussion

Collectively these results demonstrate that the combined absence of dynamins 1 and 3 has dramatic synergistic effects on the kinetics of synaptic vesicle endocytosis, but perhaps more surprisingly, show that the DKO synapses still recycled their synaptic vesicles albeit at a much reduced rate. It is unclear if the remaining endocytosis is dependent upon the presence of the low levels of dynamin 2 expressed in the cultures, or if it is completely dynamin independent. We see that the Dynamin 1 KO is defective in the post-stimulus endocytosis time constant compared to wildtype, but the size of the effect is small. This defect was not reported in the original characterization of the dynamin 1 KO, as it would not have been evident given the precision of the measurements at the time. However, the difference in the size of the effects between the Dynamin 1 KO and the DKO, clearly suggest that endogenous levels of dynamin are much greater than necessary for maintaining basic synaptic vesicle endocytic functions. Dynamin 3 is able to fully rescue the lack of dynamin 1 [25]; and the lack of it does not produce a phenotype. Therefore, it seems that dynamin 1 and dynamin 3 are interchangeable with regards to their basic presynaptic function. Compared to dynamin 2, they are more similar [36, 93] and both undergo stimulation dependent dephosphorylation. It is not The role of endogenous dynamin 2 in the presynaptic terminal remains unclear as overexpressing dynamin 2 can only partially rescue defects in the dynamin 1 KO [25] and in dynamin 1/3 DKO (see chapter 5). While this does confirm the observation that dynamin 2 is expressed at a very low level, and is not upregulated in the absence of dynamin 1 and 3 [25, 72]. However, this does not address the question if dynamin 2 has an endogenous role or is just compensating for the absence of the other isoforms. Unfortunately, the dynamin 2 KO is not viable and therefore this question has been difficult to address.

EM tomography on the dynamin 1 KO showed large grape clusters of large invagi-

nations, tipped with many clathrin coated pits. These grape clusters were seen on a subset of synaptic terminals; while in the DKO they were far more prevalent. These clusters were resolved after treatment with the sodium channel blocker TTX, which prevented activity in the culture [25,72]. While we did observe a large surface fraction in the dynamin 1 KO and DKO; it is unclear if these are the same phenomenon. Both the dynamin 1 KO and DKO recovered all the material which was exocytosed after each run. When imaging cells, they are maintained in the absence of non-stimulated activity by the glutamate receptor blockers in the media; if the recovery of the grape clusters are on a similar time-scale as our observed endocytic decays, they would have resolved before we started imaging. The presence of a high surface fraction has been seen in some but not all endocytic defects. For example the AP-2 KD [45] had high surface fractions and defective endocytosis; while, Synaptojanin KO showed no increase in surface fraction, but still had defective endocytosis [59]. Synaptic vesicle endocytosis is tightly coupled to exocytosis; the regulating factor that decides how many vesicles to endocytose however is unknown. Similarly it is thought that the surface fraction is the steady state imbalance between spontaneous exocytosis and endocytosis; however, this has been difficult to test directly. All proteins analyzed so far have some surface fraction, Vamp2, Synaptotagmin, vGlut, Synaptophysin [42,82]; leading to the hypothesis that there must be one synaptic vesicle protein that is limiting and nucleates the formation of the endocytic pit.

Previous analyses of dynamin function have relied upon dominant negative effects, such as the temperature sensitive allele in the drosophila mutant shibire [51,52] or the introduction of GTPγS [111]. Such mutants likely lock dynamin in a non-functional state around the bud neck and preventing fission. Previous studies in the lab demonstrated that synaptic vesicle endocytosis has a single rate limiting step; however, based upon this data it is unlikely that dynamin is the rate limiting factor; given its very shallow dependence on its abundance. The variability between cells

seen in chapter 4 would predict that the rate limiting step will be very sensitive to perturbations in concentration of the modulator. However, dynamin is essential for maintenance of basic endocytic kinetics at the presynaptic terminal.

4. Variability in synaptic vesicle endocytosis

Synaptic vesicle recycling is critical to ensure a ready supply of vesicles for ongoing activity. Relatively little is known about how functional properties of individual synapses differ across synapses from the same axon, although recent studies have demonstrated that release probability has a large degree of local regulation [5,12,100]. Questions of how endocytic properties vary across synapses however have not been explored. Here we sought to determine the extent to which endocytosis kinetics are determined at the single synapse versus at the cellular level and to classify the range of variations present between synapses and between cells.

Given the stochastic nature of endocytosis at the single vesicle level, we reasoned that approach these questions we would need to provide sufficient sampling from each synapse, and hence maximize the number of trials, to assemble large dataset with which to analyze the variations between runs, boutons, and cells. The low-photobleaching rate and high sensitivity of the pHluorin assay allowed us to interrogate endocytic performance repeatedly over many trials across numerous nerve terminals [8]. A single transfected neuron expressing vGlut-pHluorin typically yielded between 12–131 boutons for analysis in a field of view from which single bouton endocytic kinetics could be measured (Fig. 4.1). The stability of the system was such that up to 35 runs of stimulation and recovery could be carried out for each cell. We

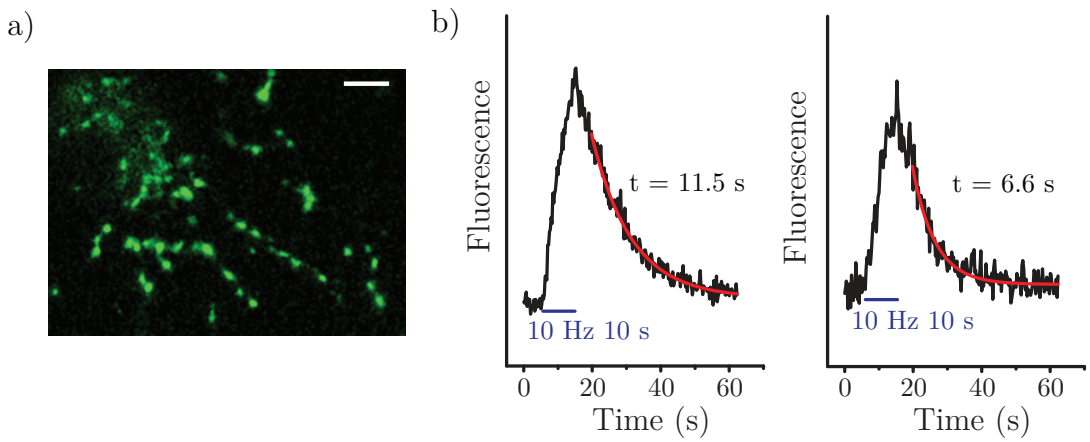

Figure 4.1: a) Representative field of synaptic boutons transfected with vGlut-pHluorin. Scale bar $10\mu m$. b) example traces with exponential fits to the fluorescence decays of a single bouton stimulated with 100AP 10Hz stimulus. Decay times are $11.5 \pm 0.5s$ and $6.6 \pm 0.4s$ respectively.

choose a 100AP 10Hz stimulus to provide sufficient amplitude of exocytosis delivering an adequate signal to noise for fitting of the endocytic time constants at single boutons in a single trial. This stimulus is in a regime that shows low stimulus dependence of the endocytic time constant (see chapter 5). The endocytic time constant is highly temperature dependent, and to avoid variations in endocytosis properties during experiments due to temperature drifts over the multi-hour experiments, the objective was heated and clamped at 30°C. Only experiments yielding stable response amplitude and kinetics across the experiment were used for analysis (Fig. 4.2b). On average the endocytic time constant was stable across the full length of the experiment, with any decreases being small compared to the variations present. The curves were fit to single exponential decays (Fig. 4.1b). The robustness of the data set was maximized by imposing stringent criteria for inclusion of individual events based on fit quality, temporal stability and signal to noise (see Methods). In total our initial analysis included 23,738 individual trial responses from a total of 1793 boutons associated with 49 neurons.

4.1 Intercellular Variation

Data associated with an individual cell is represented as a heat map, color coded to show τ_{endo} values obtained for the 300-1200 events measured across all boutons of an individual cell (Fig. 4.2c). The mean τ_{endo} for each bouton in turn allowed us to determine the variance of τ_{endo} across boutons within a given cell. For the example shown in Figure 4.2c, the coefficient of variation (CV) across boutons was ∼19%, similar to the mean intrabouton CV determined from many cells (17.5 ± 0.9% n=34 cells). Contributions to the CV are expected to arise from at least two sources: (1) for each bouton, endocytosis is likely stochastic, and therefore will lead to inherent variations that can only be averaged out with sufficient measurement repetition; (2) the characteristic τ_{endo} for each bouton may be genuinely different (a biological variation). In order to determine the relative contributions of these to the CV, we took several approaches: first we examined if the data could explain the CV by being undersampled and the stochastic basis of synaptic vesicle endocytosis. Secondly, we examined contributions to the variation due to differences in exocytosis between boutons. Lastly, we examined if there is any shared axonal properties along specific branch segments.

4.1.1 Variations in the data

We first used a boot-strap approach, whereby one tests the hypothesis that fluctuations arise non-randomly by recalculating the average CV after many random reshuffles of the data [23]. Variations across boutons due to insufficient sampling would result in a distribution of CVs obtained after reshuffling the data covering the original data set. Averaged across 500 permutations per cell the boot-strap approach predicts a CV of 9.4 ± 2.5% (standard deviation) indicating that some of the experimental average CV (17.5 ± 0.9%) likely arises from too limited a sampling of a

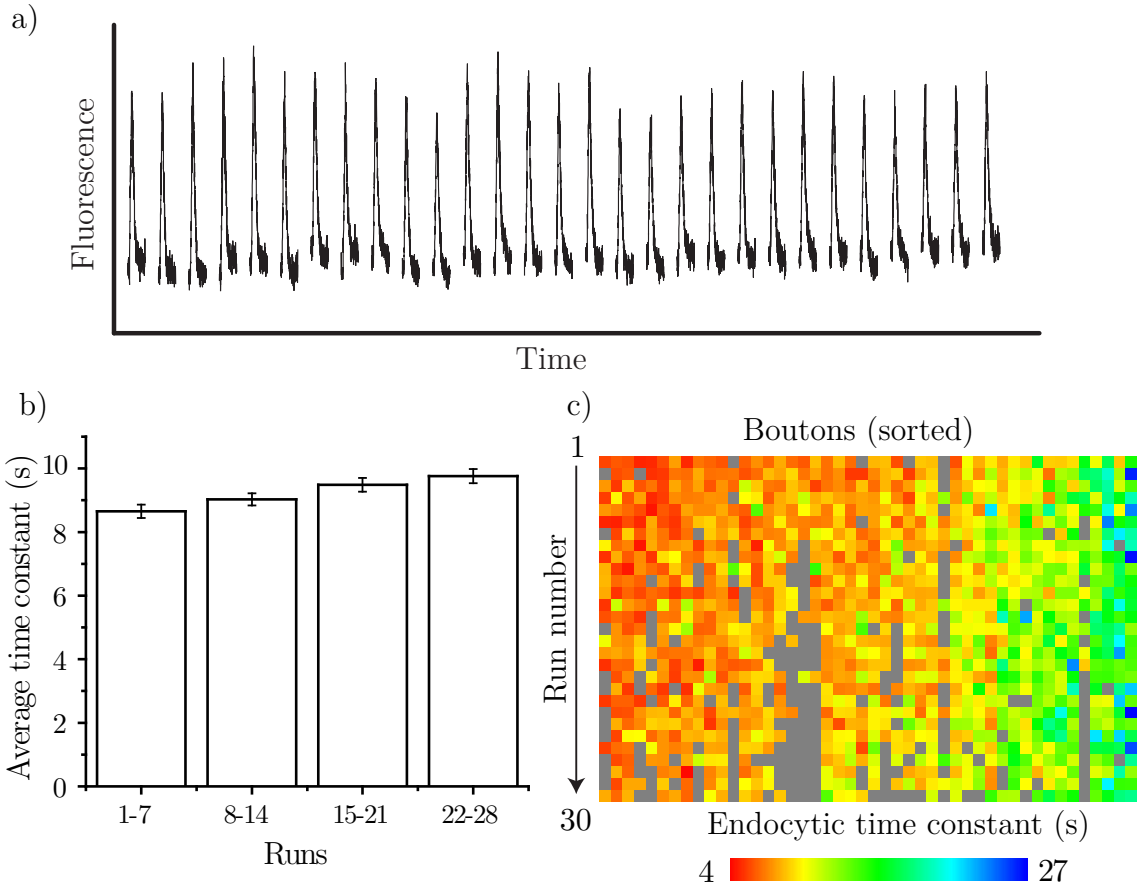

Figure 4.2: a) exo-endocytic responses from 29 consecutive runs from a single bouton with 5 min recovery between runs. b)Temporal stability of endocytosis From the experiment in Figure 1, average time constant averaged across runs, showing relative stability of endocytosis. (Means (SEM): $8.6 \pm 0.2s$, $8.9 \pm 0.2s$, $9.5 \pm 0.2s$, $9.7 \pm 0.2s$; $N \approx 250$ per bin) c) Heat map of all endocytic decays of an individual cell, color-coded from 4s (red) to 27s (blue), with grey being events that did not pass inclusion criteria. Boutons are sorted from fastest (left) to slowest (right); while runs are from first (top) to last (bottom). (29 runs, 46 boutons, 1136 events, average time constant $9.2s \pm 0.1s$).

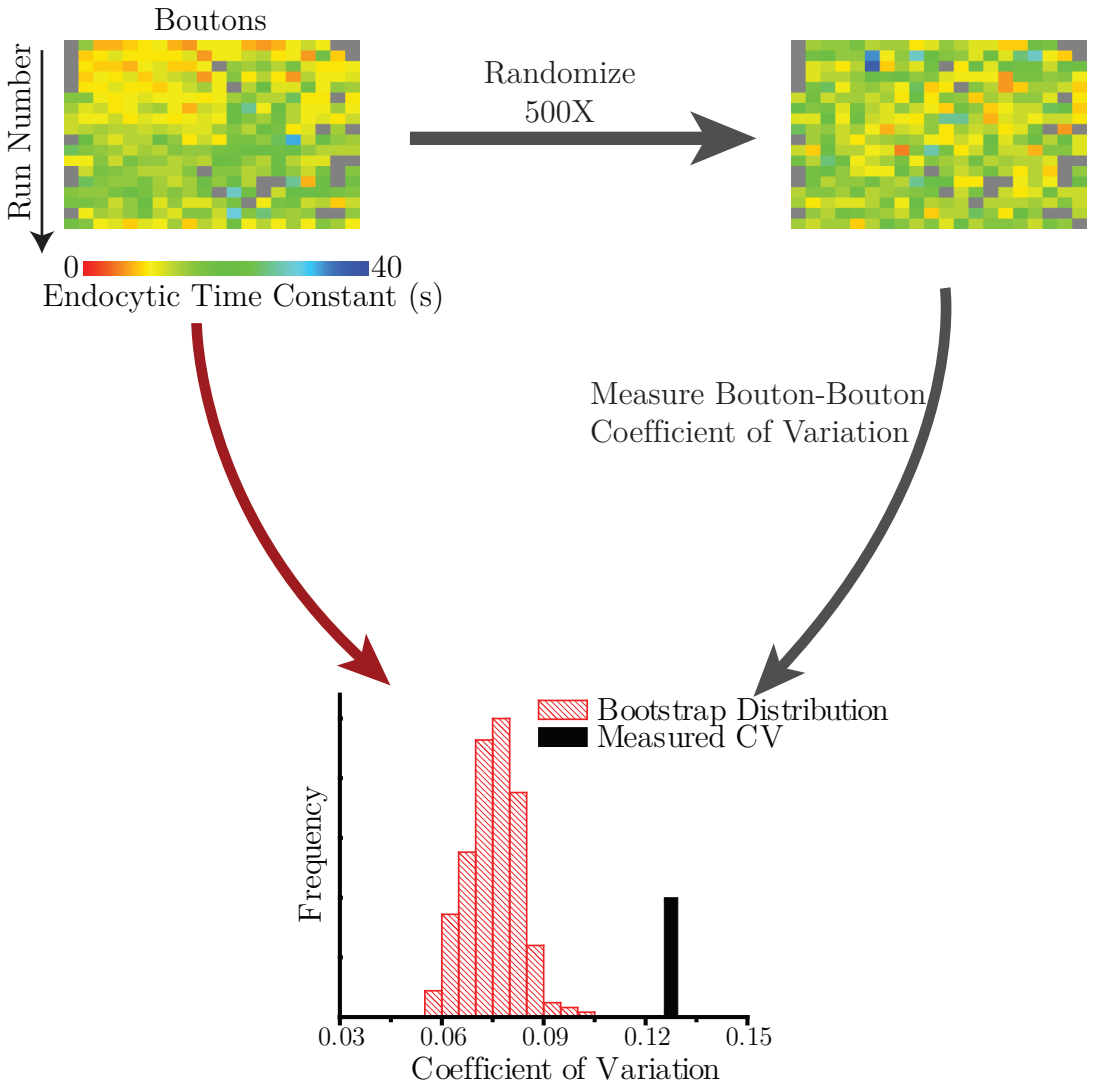

Figure 4.3: Description of the boot-strap approach of estimating undersampling in the measure of synaptic vesicle endocytic bouton events. The measured events represented in a heatmap (gray pixels represent events that did not meet fitting criteria). The order of events are randomized 500 times, and refilled into the same number of boutons with the same number of runs. The CV is calculated and the distribution of randomized CV is compared to the observed CV. In the example cell pictured bootstrap distribution observes a CV of $7.5 \pm 0.8\%$ while the observed CV is 12.6%. Illustrating that not all variations are undersampling.

stochastic process, but that the CV can not be purely explained by undersampling. We explicitly calculated, from a theoretical standpoint, the degree of fluctuation expected based upon the single vesicle description of endocytosis as an exponentially distributed stochastic process [9]. The basis was extended to a several vesicle Markov Model where each of n vesicles are internalized independently with the same stochastic parameter (see Methods). The distribution of all bouton events from individual cells was then fit to the Markov model with only two free parameters, n and $\langle \tau_{endo} \rangle$ (Fig 4.4).

The data shows that individual τ_{endo} span a wide range, from $\sim$3s to 40s. These extremes in the distribution are expected from a stochastic process, as is verified by the fact that the entire distribution is accurately fit by the n-vesicle Markov model. The models prediction of the number of vesicles internalized, 17 ± 1 (n=34 cells), compares well to our experimental estimate of 15 ± 2 for this stimulus (see Methods). The Markov model suggests that a large amount of the bouton to bouton variation could be explained just by sampling, which we will explore further with an explicit simulation.

4.1.2 Simulation of endocytosis

The second approach is based upon an apriori model of endocytosis, while the Markov model allowed us to fit our pooled bouton event data; this simulation allows us to incorporate more bouton to bouton variation in exocytic properties to try and explain more of the CV between boutons. We simulated the endocytic process and by introducing the number of vesicles for each bouton event as a random variable. N is normally distributed based upon the average number of vesicles in our data set and the average CV of the endocytic load, $61 \pm 6\%$ based upon 7 cells. This simulation predicts an expected bouton to bouton CV of $\sim$13%. This simulation is conservative, it assumes the average number of vesicles exocytosed is equal across all

boutons. Between these two approaches, most of the observed CV can be explained due to sampling issues, variations in exocytosis between bouton events, and variations in endocytosis time constants due to differences in endocytic load.

4.1.3 Variability corrections for stimulus dependence

We selected the 100AP 10Hz stimulation for the variability analysis based upon the data that the time constant was invariant with respect to the endocytic load. As we have seen in chapter 5, at 30°C there is a slight stimulus dependence that is revealed by examining individual cells. A portion of the unexplained variability in endocytosis therefore is likely due to differences in endocytic load arising from differences in release between runs and between boutons. To examine this possibility we took two approaches. First our data set contains explicit information about the variation in exocytosis amplitude across boutons and runs. This data can be used to correct for the differences in the endocytic load. When we examine all of the endocytic events from an experiment in relation to their amplitudes (Fig. 4.5a), there was a clear trend mimicking what we have found on the cell average behavior of stimulus dependent slopes. If we assume that the endocytic-load behavior is uniform across boutons and that they are all within the linear range we can fit a linear relationship to the data. The residuals (Fig. 4.5b) represent variations in endocytic time constant that are independent of the load. When we calculated the variance of the corrected data set and compared it to the original we found that the endocytosis dependence on exocytosis results in $3.1 \pm 1.1\%$ coefficient of variation (based on 7 cells, between 299–1101 bouton events). While exocytosis is a bouton specific property, a greater fraction of the variations could be explained with a bouton specific correction; however, there isnt sufficient data to measure the stimulus dependence on an individual bouton level.

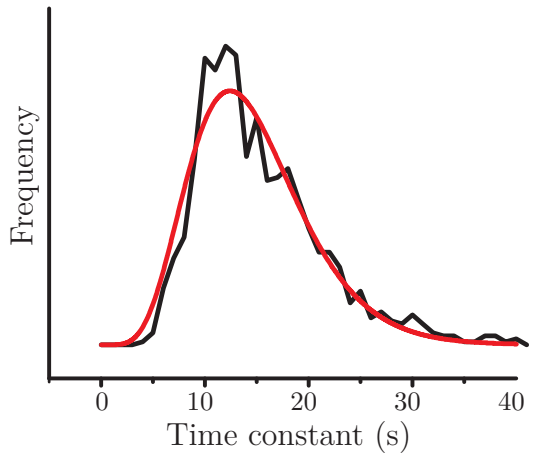

Figure 4.4: Histogram of all 832 bouton events from a single cell plotted with the maximum-likelihood fit of the Markov model (Histogram (black) mean $\langle\tau_{endo}\rangle$= 14.50 s, Model (red) mean $\langle\tau_{endo}\rangle$= 15.22 s, n=19 vesicles).

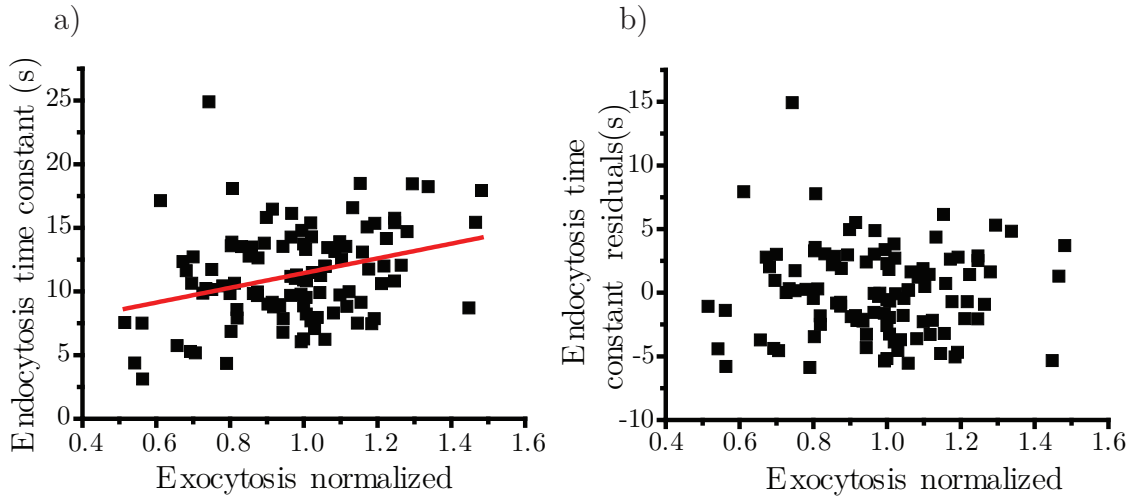

Figure 4.5: a) scatterplot of amount of exocytosis and endocytic time constant of all bouton events from a single cell. A linear fit describes the load dependence of endocytosis, as explored further in chapter 5. b) residuals from the linear fit in (a), reduces the variations in synaptic vesicle endocytosis within a cell. Variance before = 13.6 Variance residuals = 12.2%.

4.1.4 Endocytic variations along axonal branches

We showed that most of the variation in endocytic time constants between boutons is due to the sparse sampling of a stochastic process. To probe the remaining variance, we examined boutons along axonal branches to see if there was less variance along individual branches. The endocytic time constant is primarily cell wide property which spans across the long distances in the axon network. Small differences between branches might be expected. We examined the variance between the average time constant of synaptic boutons along a single axonal branch compared to the variance of the average time constant across all boutons. A similar analysis showed that there was no presynaptic release properties which localized to axonal branches [6].

We used morphological criteria based on our fluorescent images to judge if two boutons shared the same axonal branch. In general our experimental field often contained sparse networks allowing us to readily identify individual axon branches; additionally fluorescence signals can sometime be seen traveling between boutons providing further evidence that they share an axonal branch. From an analysis of 6 cells, 32 distinct axonal branches were identified. The variance along the axonal branches was normalized to the variance between all boutons of the respective cells. On average $83.4 \pm 21.9\%$ (n=32) of the variance was present between boutons along the same axonal branch compared to the entire field of boutons.

This analysis showed that there is some axonal branch identity, but it only contributes a small fraction of the bouton to bouton variability. The majority of our measured variability can be accounted for by the undersampling of a stochastic process. This result supports the idea that the endocytic time constant is a cell wide property which has only small variations in between different axonal branches, across the large distances of the axonal network.

4.2 Cell to cell variations

We concluded that most of the variation within a cell is due to undersampling, and the endocytosis time constant is primarily a cell wide property which can therefore be described on a cell wide level by a single $\langle \tau_{endo} \rangle$ value which is now sampled at the level of hundreds to thousands of bouton events. This allows us to compare $\langle \tau_{endo} \rangle$ values across many cells. Given that our data indicate that endocytosis is well characterized by a cell-wide property, we reasoned that one could obtain valid estimates from of $\langle \tau_{endo} \rangle$ using fewer repetitions (50-250 bouton events) allowing us to increase the total sample size for this aspect of the analysis. Following this reasoning we expanded the data set to a total of 84 individual cells. These data showed that unlike for individual boutons, individual cells showed a large degree of variation in $\langle \tau_{endo} \rangle$. Over the entire distribution of cells (n=84) the cell $\langle \tau_{endo} \rangle$ ranged from 5.5s to 38.9s with a CV of 41% (Fig 4.6b).

We wondered if $\langle \tau_{endo} \rangle$ might be correlated with neurotransmitter type, age in culture or history of chronic activity. Age in culture showed no significant trend in $\langle \tau_{endo} \rangle$ over the 8 day range of ages used (Fig 4.6c). We used retrospective vGlut and vGat immunocytochemistry to determine if variation in endocytosis kinetics might be correlated with the type of neurotransmitter being release (Fig 4.7a). These experiments revealed that both groups showed a wide range of $\langle \tau_{endo} \rangle$ with no statistically significant difference between the distributions (Fig 4.8). Individual neurons appear to adjust key properties associated with synaptic transmission in response to levels of chronic activity, known as a homeostatic scaling. Given the cell-wide but cell-specific character of endocytosis kinetics we sought to determine if this presynaptic parameter was under homeostatic feedback control. To test this idea $\langle \tau_{endo} \rangle$ measurements were obtained from neurons in which electrical activity had been chronically silenced for 2-8 days using TTX. We recently showed that such treatments result in acceleration in

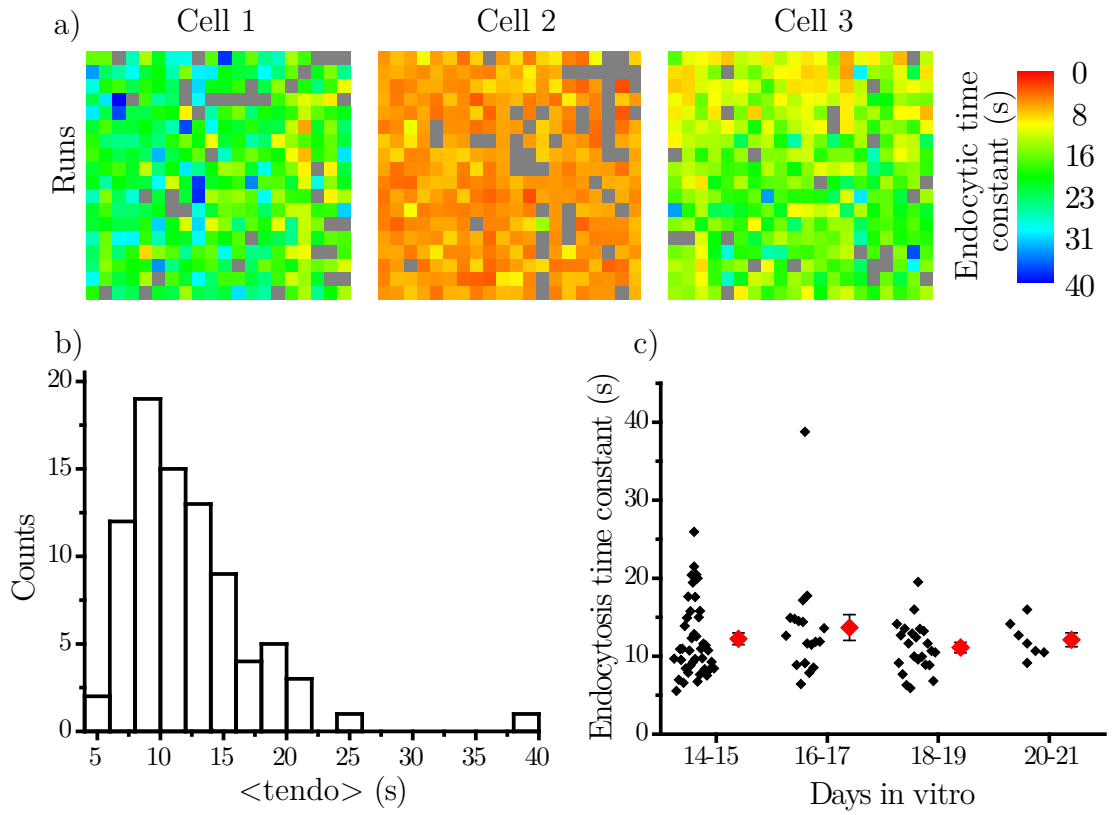

Figure 4.6: a) Heat maps of 3 different cells (truncated to 18 runs (top to bottom) and 20 boutons each). Grey represents bouton-events that did not meet inclusion criteria. (Average τ_{endo} $20.7 \pm 0.3s$, $6.3 \pm 0.1s$, $15.7 \pm 0.3s$) B) $\langle \tau_{endo} \rangle$ distribution across cells shows a range from 5.5s 39.8s (n=84 cells) c) Endocytosis is independent of days in vitro $\langle \tau_{endo} \rangle$ of cells are plotted against age of cell in vitro. Red-diamonds show the average time constant with standard error for each age, while black diamonds show each cell in the binning. $\langle \tau_{endo} \rangle$ 14-15 DIV $12.23 \pm 0.76s$, 16-17 DIV $13.67 \pm 1.65s$, 18-19 DIV $11.10 \pm 0.67s$, and 20-21 DIV 12.10 ± 0.89s. No statistically significant difference in the distribution of endocytic time constants between cultures imaged days 14–15,16–17, 18–19, or 20–21. (KS–test, p=0.14, p=0.48, p=0.57).

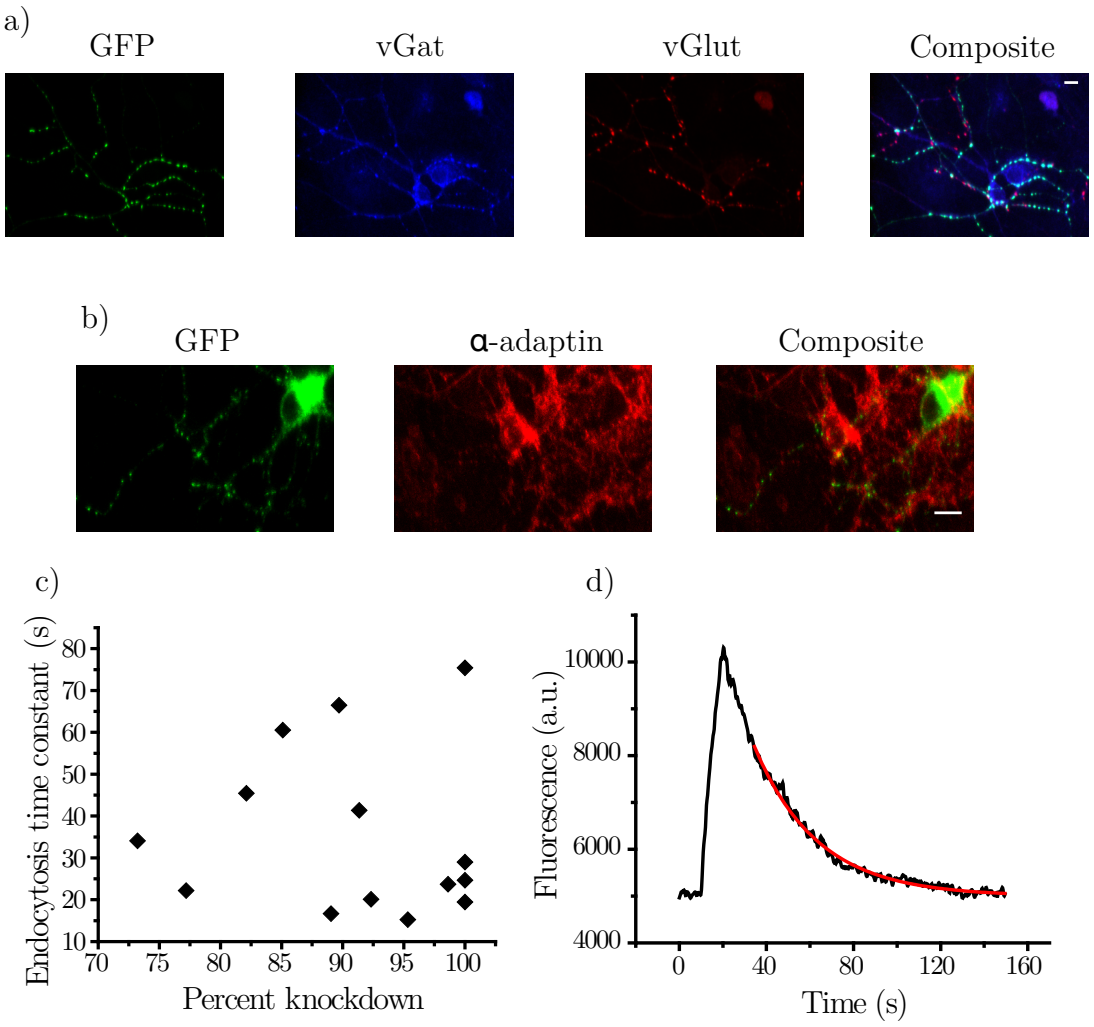

Figure 4.7: a) Retrospective vGlut/vGat staining example. Example triple-staining a physin-pH transfected neuron: anti-GFP(green), anti-vGat(blue), and anti-vGlut(red). In the example picture the GFP-positive cell was determined to be an inhibitory cell. Scale bar represents 10um. b) AP-2 knockdown staining example Example of staining for a AP2 knockdown: anti-GFP (green) and anti-α-adaptin. The example pictured has a 91% knockdown. Scale bar represents 10um. c) $\langle \tau_{endo} \rangle$ is independent of AP-2 knockdown level Plot of percentage of AP2 knockdown in relation to the average endocytosis time constant. Showing no clear relationship of endocytic variability and knockdown. d) AP-2 knockdown example trace Example trace of endocytosis in AP2-Knockdown cell in response to 100AP 10Hz stimulus. Endocytic time constant 29.0 ± 0.6s at 30°C

exocytosis kinetics and increases in the size of the synaptic vesicle recycling pool [46], however these experiments showed that the endocytic profile of cells appears invariant with respect to the history of chronic activity, irrespective of neurotransmitter type (Fig 4.8).

Finally we examined whether variability in $\langle \tau_{endo} \rangle$ would be sensitive to perturbations known to dramatically slow endocytosis. We made use of shRNA-mediated knockdown of the clathrin adaptor AP-2 (Fig 4.7b), resulting in 3-fold slowing of SV endocytosis [45] (Fig 4.7c,4.8), consistent with the observations that SV endocytosis is largely a clathrin-mediated process. As with WT neurons, we found significant variability in $\langle \tau_{endo} \rangle$ from cell to cell (WT $CV_{\langle \tau_{endo} \rangle} = 41\%$ (95% confidence interval 34%-49%), AP-2 KD $CV_{\langle \tau_{endo} \rangle} = 56\%$ (95% confidence interval 24%-82%) [103]) (Fig. X) that was unrelated to the degree of knockdown (Fig S5). Thus the mechanism of the cell to cell variations in endocytosis remains intact despite dramatic slowing of the endocytic process.

4.3 Discussion

Based upon all of these approaches we determined that the vast majority of the variation between boutons can be explained due to the stochastic nature of endocytosis, sampling, variations in exocytosis between the boutons, and small variations between axonal branches. Therefore the endocytic time constant is fairly homogenous across all boutons within the same cell. We observe ∼17% CV between boutons, while the model of sampling expects ∼13%, additionally, variations in exocytosis affecting endocytosis contributes 3% CV to our expected number. We saw that along axonal branches there is up to 17% lower variance between boutons along the same axon; while a small difference, it does support the idea of a diffusible factor setting the endocytic time constant across the entire axon, and these axonal variations are resultant

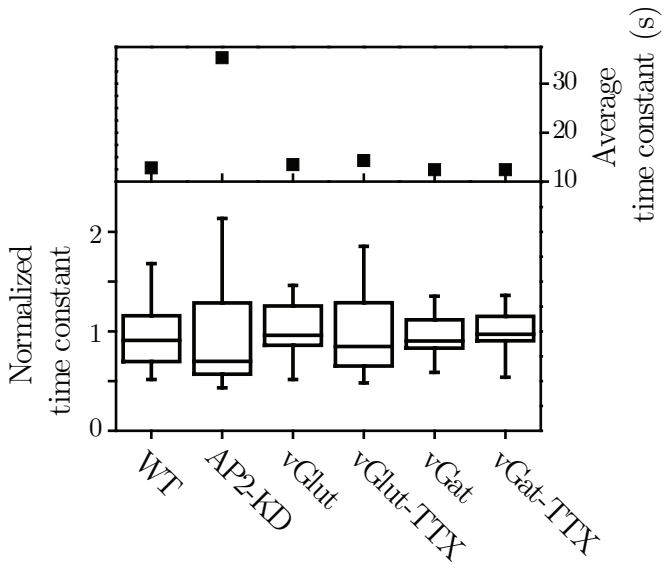

Figure 4.8: Distribution and $\langle \tau_{endo} \rangle$ of WT, AP2-KD, vGlut-positive, vGlut-positive TTX silenced, vGat- positive and vGat-positive TTX silenced cells based upon post-experiment immunofluorescence staining. Normalizing the distributions to their mean showed that there is no significant difference in the spread of the distribution for AP2-KD cells compared to WT (KS-test p=0.29). Silencing cultures with TTX for 2-8 days showed no significant difference in their distributions (KS-test p=0.24 vGlut, p=0.69 vGat). vGlut, vGat segregation showed no significant difference in their distributions (KS-test p=0.28). (Box-whisker plots showing $5\%-25\%-50\%-75\%-95\%$) is plotted. (WT n= 84, AP2-KD n=14, vGlut n=10, vGlut-TTX n=14, vGat n=16, vGat-TTX n=11 cells) Cell averaged time constants WT $12.3 \pm 0.6s$, AP2-KD $35.3 \pm 5.3s$, vGlut $13.4 \pm 0.8s$, vGlut-TTX $14.3 \pm 1.5s$, vGat $13.4 \pm 0.9s$, and vGat-TTX $12.4 \pm 0.9s$.

of small local variations across the spatially large axonal network. The data places an upper bound on the amount of biological variation between boutons ∼10% (Sampling, Exo-dependence). In contrast our analysis of $\langle \tau_{endo} \rangle$ across 84 cells indicates that there is a 4-fold greater variability in this parameter across cells. Thus endocytic performance is primarily a cell-wide parameter. Given that exocytosis properties have been shown to vary significantly across synapses [6], these results suggest that endocytosis is largely uncoupled from aspects of exocytosis. Similarly, the type of neurotransmitter transporter present in the cell(excitatory or inhibitory) shows no systematic differences in their endocytic properties. Consistent with these findings we found that chronic silencing of neurons, previously shown to lead to up-regulation of both pre [46, 65] and postsynaptic [101] aspects of synaptic transmission, did not lead to measurable changes in the $\langle \tau_{endo} \rangle$. This complete disconnect between exocytic modulation and recycling modulation poses the question of how the endocytic properties are modulated.

Our data indicate that the key parameter describing endocytic performance is set at the single cell level, perhaps reflecting a regulatory program related to specific, but as yet unidentified elements of the endocytic machinery. Perturbing a protein that participates in endocytosis (AP-2) dramatically slows endocytosis but the variability scales with the slowing of the time constant. Despite its modulatory potential, the lack of change in modulation with endocytic defects (AP-2), or any subdivision of modulation suggests that the regulation is controlled at a very fundamental level which likely is not related to an active feedback. The identity of this modulatory system remains unknown however its existence predicts a potentially powerful means of controlling presynaptic performance.

5. Ca^{2+} Dependence of Endocytosis

The effects of Ca^{2+} and stimulation on endocytosis has been examined previously in the lab [8, 84] and by others [30, 104, 108]. Previous studies have taken many different approaches, examining changes with endocytic load, different extracellular Ca^{2+} concentration, different stimulus frequencies, and changing intracellular Ca^{2+}. The different approaches have arrived at different conclusions: slowing of endocytosis by elevated Ca^{2+} and low Ca^{2+} as well as endocytosis that is independent of Ca^{2+} or stimulation. With the improved temporal resolution and signal to noise of vGlut-pHluorin as well as the better understanding of cell to cell variations we reexamined the stimulation/Ca^{2+} dependence of endocytosis kinetics. As a surrogate for direct changes Ca^{2+}, we chose to modulate the length of stimulation while maintaining a constant frequency. For stimuli at 10Hz we found a simple relationship between the length of the stimulus (number of action potentials) and the endocytic time constant. For a range of stimuli from 10AP to >100AP at 10Hz stimulus, this relationship can be approximated as a linear dependence, see figure 5.1 and 5.2a. Previously we found that there were two phases of endocytic behavior, one below a critical endocytic load and one beyond it, where we proposed that the endocytic machinery was in saturation for larger loads, and the endocytic time constant was invariant for smaller loads [8]. There are two discrepancies between the observed linear relationship and the saturation model of endocytosis; first, below the critical endocytic load no relationship was found between the time constant and the load; second, no equivalent transition

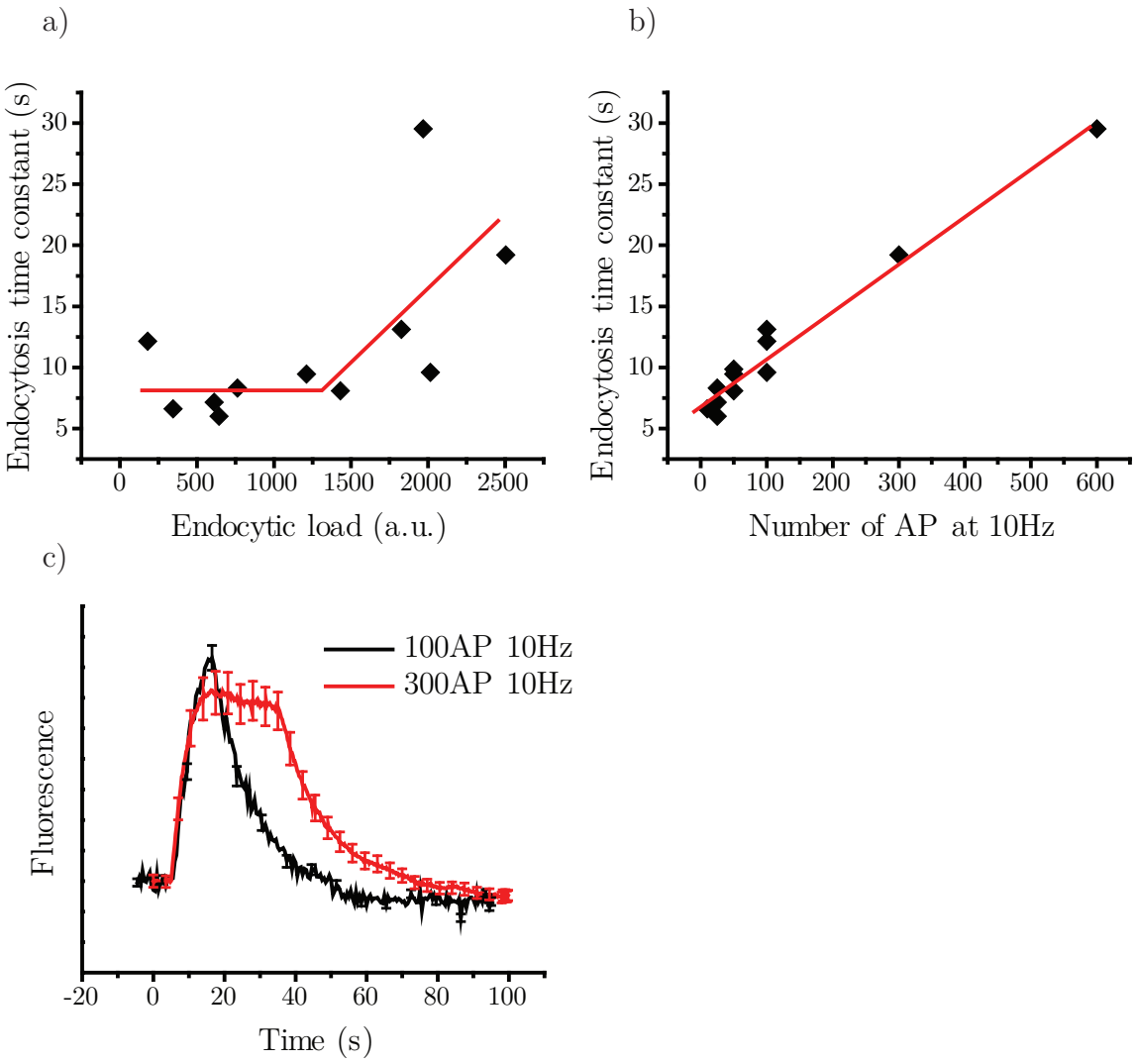

Figure 5.1: a) example from a single cell plotting all runs at 30°C, by its endocytic load versus the measured endocytic time constant. As was previously shown this results in an invariant regime and a saturation regime. b) same example cell in (a) plotted versus number of AP at 10Hz, demonstrating a linear relationship. c) the difference between endocytic load and number of AP arrises with large stimuli, that plateau before the end of stimulation. This distorts the endocytic load curve.

is seen in the endocytosis-stimulus dependence. However the average change of endocytosis constant as a function of the total number of action potentials is rather subtle compared to the cell-to-cell variability and could easily have been missed. The second question arises from the difference between the considered variables: the first study uses the endocytic load, i.e. how much of the functional reporter had accumulated on the surface by the end of the stimulus and the beginning of the post-stimulus endocytic decay, while our current analysis uses the number of action potentials. For small stimuli these variables are closely matched; however, for large stimuli there was a disconnect between the two. For large stimuli the endocytic load reaches a near steady state value. Under these conditions however as the number of stimuli is increased, our linear fit shows that endocytosis will continue to slow. This creates an apparent break in the endocytosis versus load curve (Fig. 5.1). Thus this compression of a large range of stimuli to small variations in the endocytic load can explain why a second saturation phase was seen in the previous study, while it is not seen in our current analysis.

5.1 Ca^{2+} Dependence at 30°C

As discussed in the previous chapter the 100AP 10Hz time constant is highly variable from one cell to the next. We therefore examined if this stimulus dependence of endocytosis is also variable and/or if the parameters of the dependence might contribute to the variance in the 100AP 10Hz endocytosis time constant. To examine this issue we repeatedly measured cells at 25, 50, 100AP 10Hz stimulus and fit a linear relationship for the endocytosis time constant as a function of stimulus number to yield an intercept (the predicted value of τ_{endo} for the lowest possible stimulus) and a slope (Fig 5.2a). From an average of 44 cells, the average intercept was 4.3 ± 0.6s with a CV of 52%. The average slope was 0.053 ± 0.008s/AP with a CV of 100%

(Fig. 5.2b). Here we see both the intercept and the slope contain the variance that is present in the 100AP 10Hz time constant, and that there is no correlation between the two parameters.

Previous studies suggested that Ca^{2+} is the variable that sets the saturation parameters [8, 40]. To test if Ca^{2+} impacts the linear relationship between number of stimuli and the τ_{endo} we changed the extracellular Ca^{2+} concentration from 2mM to 4mM. To correct for the increased exocytosis we plotted the amount exocytosed and used only short stimuli <10s where there was very little endocytosis during stimulation (see dynamin methods). Each cell was probed both at 2 and 4mM Ca^{2+} concentrations, an example pictured in figure 5.2c shows both a steeper slope and a reduced intercept. On average over 9 cells there was no significant difference in the intercept but the slope is significantly steeper for 4mM Ca_e^{2+}, the ratio of the 2mM to the 4mM slope was 0.42 ± 0.16, see figure 5.2d. This indicates that Ca^{2+} influx rather than load is the determining variable for modulation τ_{endo}, as for equivalent load the endocytic time constant is different when we compare 2mM and 4mM external Ca^{2+}. These data support the idea that Ca^{2+} rather than load is the variable triggering the modulation.

While we have focused our experiments on the 10-100AP stimulus range at 10Hz, we wanted to test experimentally the prediction that a 1 AP stimulus would lead to the fastest value of τ_{endo} for a given cell. Figure 5.4b shows an example of a single AP exocytic response and endocytic recovery. The fit to the decay phased gave $\tau_{endo} \sim$12s while for the same cell the intercept from the linear fit to the stimulus dependence was 6s. This large discrepancy between the measurements for single AP and the linear prediction was born out across a population of neurons where, on average (n=10 cells), the 1AP time constant is 42% slower than what the intercept predicts. This indicates that there was a second stimulus small range is difficult to probe due to low signal to noise and only few discrete steps in the stimulation. To test if this acceleration phase

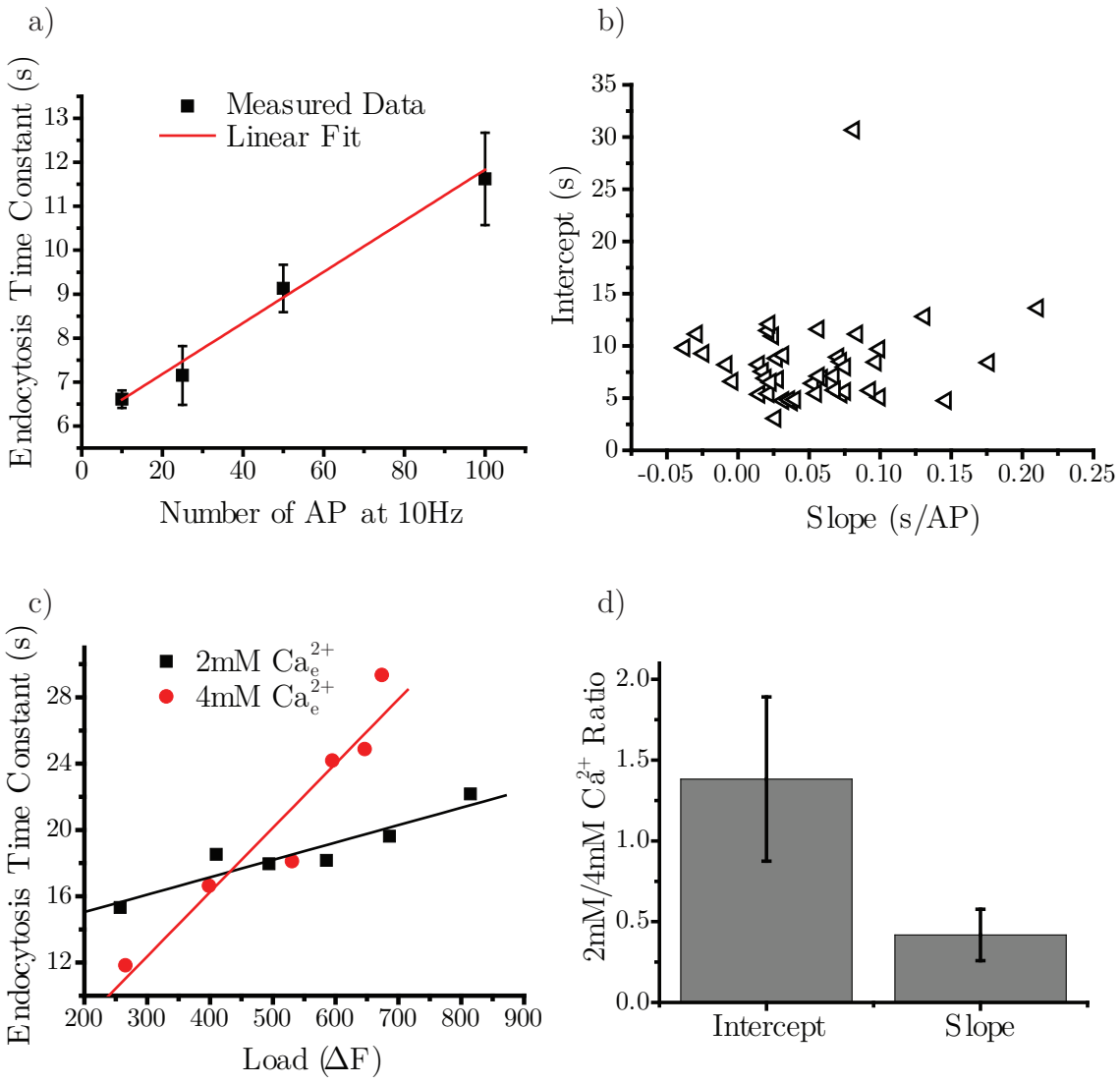

Figure 5.2: a) an example cell probed multiple times at 10, 25, 50, 100AP at 10Hz at 30°C, fit with a linear dependence a slope of 0.058 ± 0.004s, intercept of 6.02 ± 0.11s. b) across 44 cells, the slope (s/AP) versus the intercept (s) are plotted. There is a CV of 100% in the slope, 52% in the intercept. Average slope 0.053 ± 0.008s/AP, intercept 4.3 ± 0.6s c) an example cell probed at 2 and 4 mM external Ca^{2+} across a similar load. Slope of 2mM is 0.01 ± 0.002s/load, 4mM is 0.04 ± 0.01s/load. Intercepts of 2mM is 13.0 ± 1.2s, 4mM is 0.74 ± 3.3s. d) across 9 cells the ratio of the 2mM/4mM external Ca^{2+} slope and intercept. The slope is significantly different from 1, (one sample t-test $p < 0.01$)

could also be Ca^{2+} dependent we decoupled the exocytosis and endocytosis Ca^{2+} sensitivity by loading neurons with the Ca^{2+} buffer EGTA-AM. The release site is thought to be closely coupled to the site of Ca^{2+} influx [14,32] while the endocytic site is expected to be more peripheral [62, 81]; therefore one expects the EGTA-AM will change the effective Ca^{2+} for endocytosis more than that for exocytosis. This allows us to probe effectively lower intracellular bulk Ca^{2+} while maintaining exocytosis and hence a larger signal to noise. Figure 5.4d shows the acceleration of endocytosis is more prominent in the EGTA loaded condition, over a similar range of exocytosis.

We have shown two different phases of the Ca^{2+} dependence of synaptic vesicle endocytosis, an acceleration phase for very small stimuli and a slowing phase for larger stimuli. Previous studies had conflicting results on the Ca^{2+}/stimulus dependence of endocytosis. One study agrees with the acceleration phase showing that for very low Ca^{2+} endocytosis is inhibited [108]. Two other studies found that the single AP τ_{endo} was similar to that for larger stimuli [8, 30]. However we feel that the combination of slowing for larger stimuli, acceleration over the first few AP as well as the fact that lower temperatures reduces the acceleration phase, this effect could easily have been missed in previous studies. These two regimes, acceleration and slowing, are distinct at 30°C, where the acceleration phase is dominant for very small stimuli (¡10AP) and the slowing phase is dominant for larger stimuli. The balance between these two phases implies that there is an ideal stimulus that optimizes the endocytic time constant. To probe the physiological significance of this balance we examined the stimulus-dependence of τ_{endo} at physiological temperatire, since the Ca^{2+} influx, extrusion, and buffering are all known to be highly-temperature sensitive.

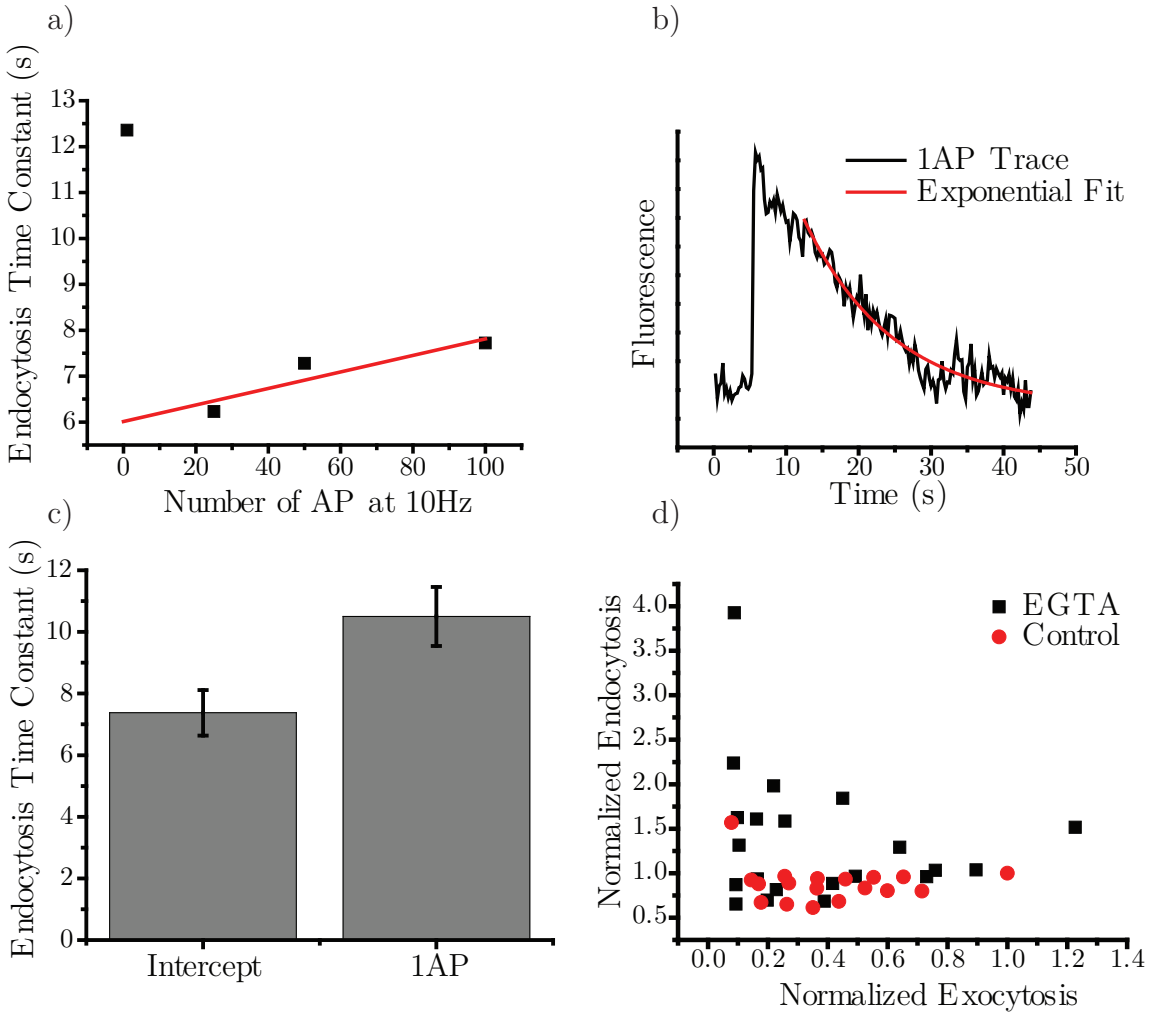

Figure 5.3: a) an example cell probed at 1, 25, 50, 100AP at 10Hz at 30°C, with a linear fit to the 25, 50, 100AP data. b) example trace of vGlut-pHluorin response to 1AP stimulation, with endocytosis fit, time constant 12.36 ± 1.1s c) across X cells, comparing the intercept fit to 25, 50, 100AP 10Hz data compared to 1AP trials. The difference is significant two sample t-test $p < 0.04$ n=10 cells. d) cells probed before and after loading with 100uM EGTA-AM 90s. Each cell is normalized to their 100AP 10Hz data point. The distribution of endocytic time constants is significantly different ks-test $p < 0.002$ n=6 cells.

5.2 Physiological Ca^{2+} Dependence

A number of presynaptic properties are well-known to be temperature sensitive: the width of the action potential [37]; the rate of exocytosis [27, 61] and the rate of endocytosis [8,61,74]. Therefore when examining the balance between two competing effects, such as the slowing and acceleration of synaptic vesicle endocytosis, it is critical to examine this at physiological temperature. The amount of exocytosis was reduced at 36.8°C, see figure 5.5a, presumably due to a narrowed action potential. The average time constant was accelerated from 30°C to 36.8°C, for a 100AP 10Hz stimulus from 12.3 ± 0.6s (n=84) to 7.55 ± 1.24s (n=10 cells). Exocytosis, reported as the fraction of the recycling pool released by 100AP 10Hz stimulation, decreased from $24 \pm 4\%$ to $19.3 \pm 2.02\%$ (n=8) when shifting from 30°C to 36.8°C.

We measured τ_{endo} for a series of stimulus lengths at 10Hz and found two phases, first endocytosis was accelerated in the 5 to 25AP regime, after which endocytosis proceeded to gradually slow. Compared to 30°C, the acceleration phase was more prominent and extended to larger stimuli. There was a clear minima for τ_{endo} around 25AP. The range of modulation between the minimum and maximum corresponded to an acceleration of $66 \pm 15\%$ (n=8 cells) (Fig. 5.4b). The endocytic minima that we see at physiological temperature, implies that single action potentials have the slowest endocytosis of all stimuli. Physiological firing patterns often have small interspersed bursts of action potentials rather than long constant frequency trains. Compared to firing lone action potentials a small burst will have accelerated endocytosis. We next designed experiments to determine if acceleration of the endocytic response would persist during pauses between bursts and if so for how long. To examine this issue we used the protocol depicted in Figure 5.5. We stimulated neurons with five bursts of 5AP (at 10Hz), spaced 15, 20, and 30s apart (Fig. 5.5) and measured τ_{endo} following each burst. These data showed a clear acceleration across bursts proved the inter-

burst interval was less than 30 s and implies that the impact of calcium on endocytosis persists for long time periods.

As the acceleration phase of endocytosis was very pronounced at physiological temperature we wondered how the slowing phase would behave compared to cooler temperatures. To probe this we examined τ_{endo} for both 100AP and 300AP at 10Hz. Endocytosis slowed from 7.83 ± 1.15 to 10.46 ± 2.36s from 100AP to 300AP at 10Hz from (n=6 cells). These data show that the slowing phase of endocytosis is still present at physiological temperature. At present it is unclear if the slowing phase has a similar persistence time to the acceleration phase.

5.3 Ca^{2+} sensor

We have shown that there is a clear Ca^{2+} dependence of endocytosis which is prominent at physiological temperature, with a persistence of at least 20s. This persistence time is much longer than the typical clearance time for intracellular Ca^{2+} following a burst of stimuli. Thus it seems likely that the calcium-mediated acceleration is being driven by a signaling system driven by Ca^{2+}. One possible mechanism would be through the Ca^{2+} dependent phosphatase calcineurin which is known to dephosphorylate a number of endocytic proteins, the dephosphins [21,77] in an activity-dependent manner. Dynamin, one of the known dephosphins, is rapidly dephosphorylated after calcium elevation and slowly rephosphorylated over 40s time period [57] similar to the time scale of the persistence of the acceleration in τ_{endo}. Calcineurin has been proposed as a Ca^{2+} sensor for endocytosis; however, direct study of its effects on endocytosis has been complicated by its many interactions [47]. The specific dynamin phosphorylation sites have been mapped [90] although the significance of the phosphorylated state has remained unclear. To test if the phosphorylation state of dynamin could be part of the mechanism of endocytic acceleration we took advantage

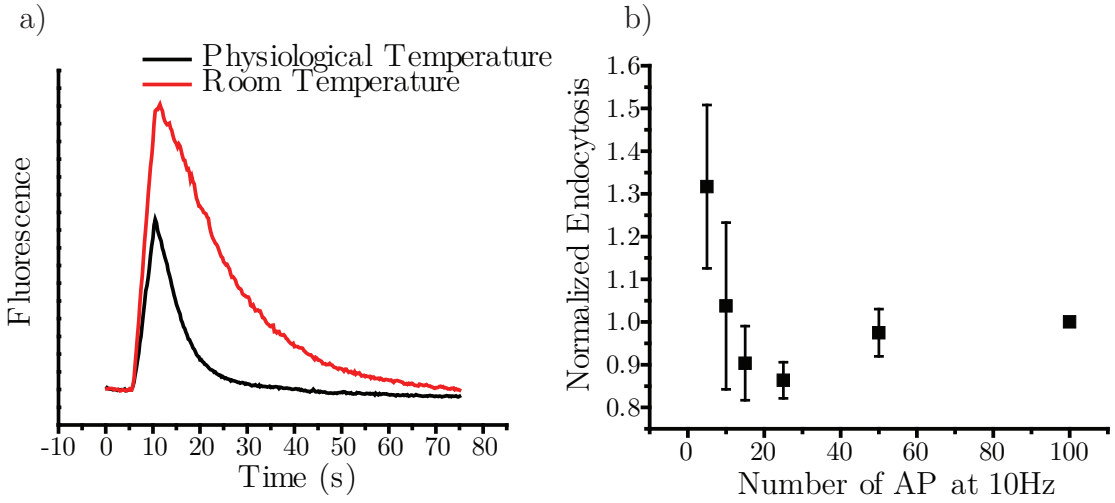

Figure 5.4: a) an example cell showing differences at physiological temperature and room temperature, 150AP 30Hz stimulation. Room temperature time constant = 15.0 ± 0.1s; physiological temperature time constant = 5.8 ± 0.04s, b) at physiological temperature, probing 5, 10, 15, 25, 50, 100AP at 10Hz, normalized for 100AP 10Hz tau for each cell, showing the acceleration of endocytosis. n=8

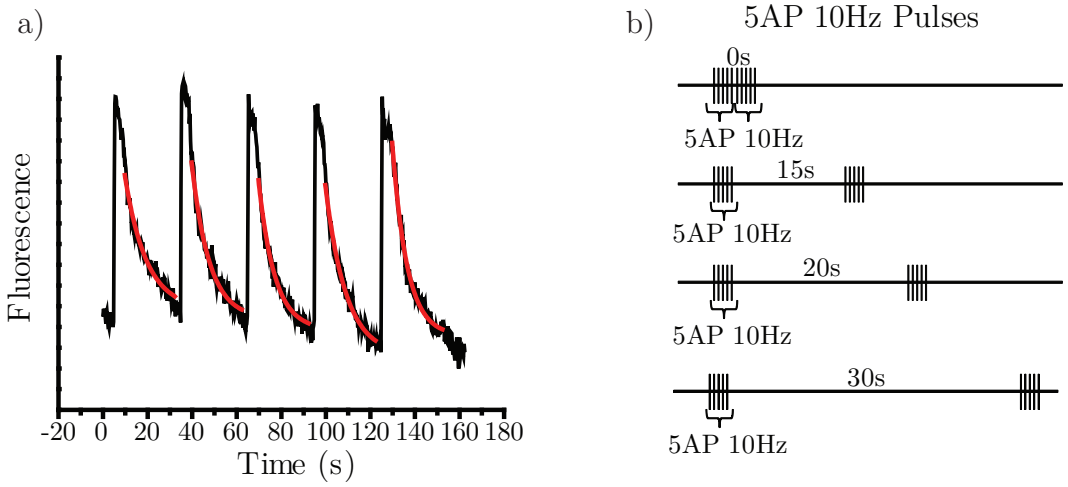

Figure 5.5: a) a train 5 pulses of 5AP 10Hz spaced 30s apart from one cell averaged over many runs, each decay is fit with an exponential decay. Endocytosis time constants = 9.7 ± 0.8s, 7.9 ± 0.5s, 7.2 ± 0.4s, 9.2 ± 0.5s, 6.7 ± 0.3s. b) to examine the persistence time of the acceleration of endocytosis 4 different temporal spacings were examined on a series of pulses 0s, 15s, 20s, 30s, spacing of 5AP 10Hz.

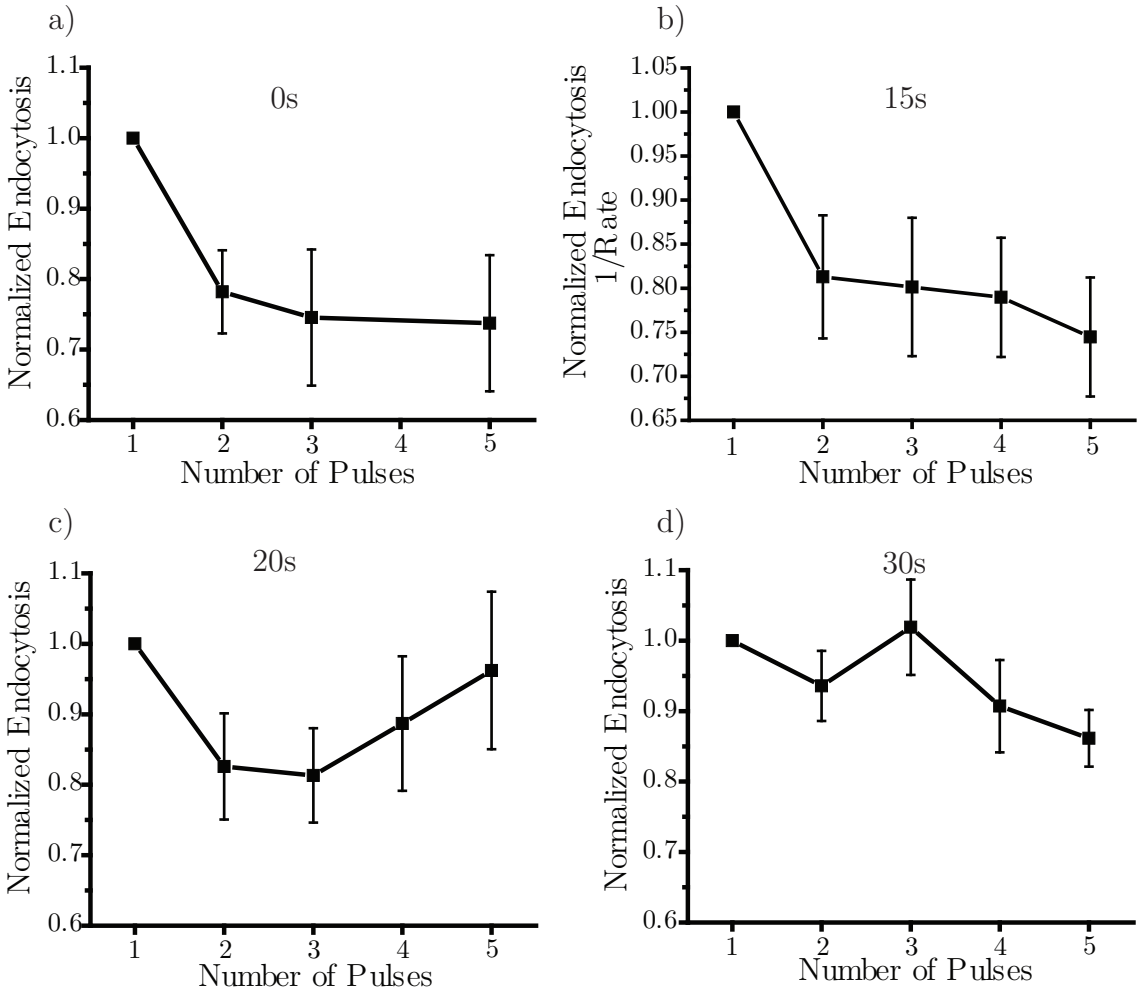

Figure 5.6: a) data from figure 5.4, 8 cells normalized to 5AP 10Hz data, shows significant acceleration of endocytosis. b) 15s spacing with linear fits for the decays, plotting 1/Rate of endocytosis, showing significant acceleration of endocytosis from the first pulse. 11 cells, $p < 0.03$ one sample t-test c) 20s spacing, fit with exponential time constants, pulses 2 and 3 are significantly accelerated compared to the first pulse $p < 0.05$ one sample t-test, 9 cells d) 30s spacing with exponential fits, only the 5th pulse is significantly accelerated compared to the first pulse $p = 0.04$. 9 cells

of the ability to carry out rescue experiments in the dynamin 1/3 DKO mice. We used two different phospho-mutant versions of dynamin 1; either a phosphodeficient state (S774A/S778A) phosphomimetic state S774D/S778D. At physiological temperature, the dynamin 1/3 DKO had a similar defect to that seen at cooler temperature. Importantly this endocytic defect could be fully rescued with wild type dynamin 1 (see figure 5.7a).

As our Ca^{2+} dependence of endocytosis experiments above were carried out in rat hippocampal neurons, we repeated these measurements in wild type mouse cortical cultures (the neurons used for the dynamin KO studies). These experiments showed both the acceleration and slowing phenotypes observed earlier in rat hippocampal cultures. The range of modulation between 10AP and 25AP at 10Hz was an acceleration of $34 \pm 18\%$ (n=5 cells) (figure 5.7b), with a 100AP 10Hz time constant of 9.3 ± 0.5s (n=10 cells). Dynamin 1 has two known splice sites on in the middle domain and one in the PRD, we expressed the a long spliceform (ba) and a short form (bb) known to bind calcineurin. Both splice forms were able to restore the Ca^{2+} dependence of ?endo in the dynamin DKO (Fig. 5.7b/d). However when rescuing the dynamin DKO with the phosphomimetic dynamin 1 (in this case the long spliceform) failed to show either an acceleration phase or any Ca^{2+} dependence (change of $0 \pm 15\%$ n=8). Additionally the average value of τ_{endo} (100AP 10Hz) was slowed to 14.5 ± 1.6s (n=12). Rescues with the phosphodeficient dynamin 1 (long spliceform) showed no statistically significant acceleration of endocytosis between 10AP and 25 AP of $11 \pm 15\%$ (n=6). However, unlike the phosphomimetic, the phosphodeficient mutant had an average τ_{endo} (100 AP, 10 Hz) similar to that of WT (9.4 ± 1.1s n=6). Thus both the phosphomimetic and phosphodeficent mutants abolish any acceleration of endocytosis for small stimuli. Rescues with a full-length wildtype dynamin 1 showed a similar Ca^{2+} dependence to controls. In summary the phosphomimetic version of dynamin 1 behaved as if there never was an acceleration while the phos-

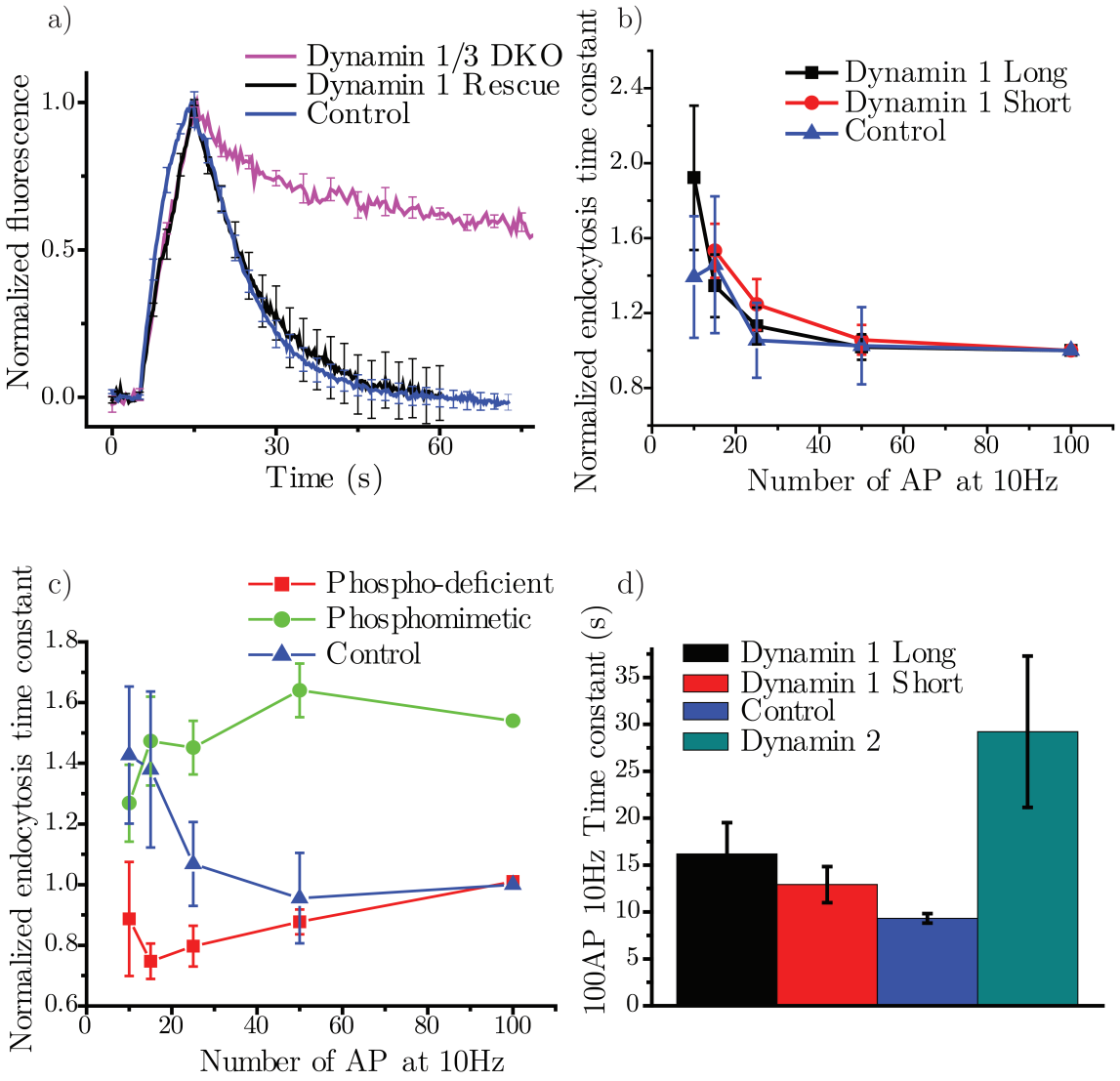

Figure 5.7: a) 100AP 10Hz stimulation of dynamin 1/3 DKO, Dynamin 1 rescue expressed in DKO, or the dynamin 1 Het dynamin 3 KO control genotype. b) examining the rescue of DKO with the long and short spliceforms of dynamin 1. All data is normalized to their 100AP 10Hz, n=9 long, 7 short, 5 control. c) Rescue with the phopho-deficient, S774/8A, or the phosphomimetic S774/8D of dynamin 1, normalized to the control 100ap 10hz data. the phosphomimetic 100ap 10hz is significantly slower than control KS test $p < 0.003$. Neither mutant shows the similar Ca^{2+} dependence of control. d) The 100ap 10Hz time constants of the rescue with dynamin 1 isoforms and dynamin 2. Dynamin 2 is significantly different from control ks-test $p < 0.0004$; Dynamin 1 long is not significantly different.

phodeficient version of dynamin 1 behaved as if the cell was permanently accelerated. These data strongly support the idea that dynamins stimulus-triggered dephosphorylation is the underlying mechanism mediating the acceleration of endocytosis. We also examined Dynamin 2s ability to rescue the DKO. Dynamin 2 also does not have the same stimulus dependent phosphorylation sites as dynamin 1 [56]. Our experiments showed that although dynamin 2 was able to partially rescue the 100AP 10Hz τ_{endo} (Fig. 5.7d) it did not show any statistically-significant acceleration ($10 \pm 18\%$ at 15AP n=8). This supports the idea that the acceleration of endocytosis is dependent upon the phosphorylation state of dynamin; and suggests one of the limitations of dynamin 2s ability to rescue is the lack of the appropriate phosphorylation sites.

Dynamins proline rich domain, which contains serines 774 and 778 binds the F-bar protein syndapin (pacsin) in a phosphorylation dependent manner [3, 17]. Syndapin is thought to play a role in synaptic vesicle endocytosis [1]. There are 3 syndapin genes in mammals, with syndapin I being the primary neuronal isoform. Previous studies showed that syndapin 1 KO have only subtle phenotypes however measurements of endocytosis kinetics in the regime where we see acceleration were not carried out [1]. We investigated whether removing Syndapin 1 would phenocopy the dynamin phosphomimetic mutant using an shRNA-mediated knockdown approach. For each experiment we determined the efficiency of our shRNA-mediated ablation using retrospective immunocytochemistry against Syndapin I compared to untransfected cells in the same field of view. On average shRNA transfection resulted in a $79.4 \pm 0.1\%$ knockdown of Syndapin I expression in primary dissociated hippocampal neurons. The value of τ_{endo} for 100AP (10Hz) for the Syndapin I KD was similar to that of WT (9.3 ± 1.1s n=9 compared to 8.9 ± 1.6s n=8). Examination of the stimulus-dependence however showed that it exaggerated and shifted the acceleration phase to a range of larger stimuli (Fig 5.8b).

We reason that since the KD is incomplete and there is possibly both syndapin

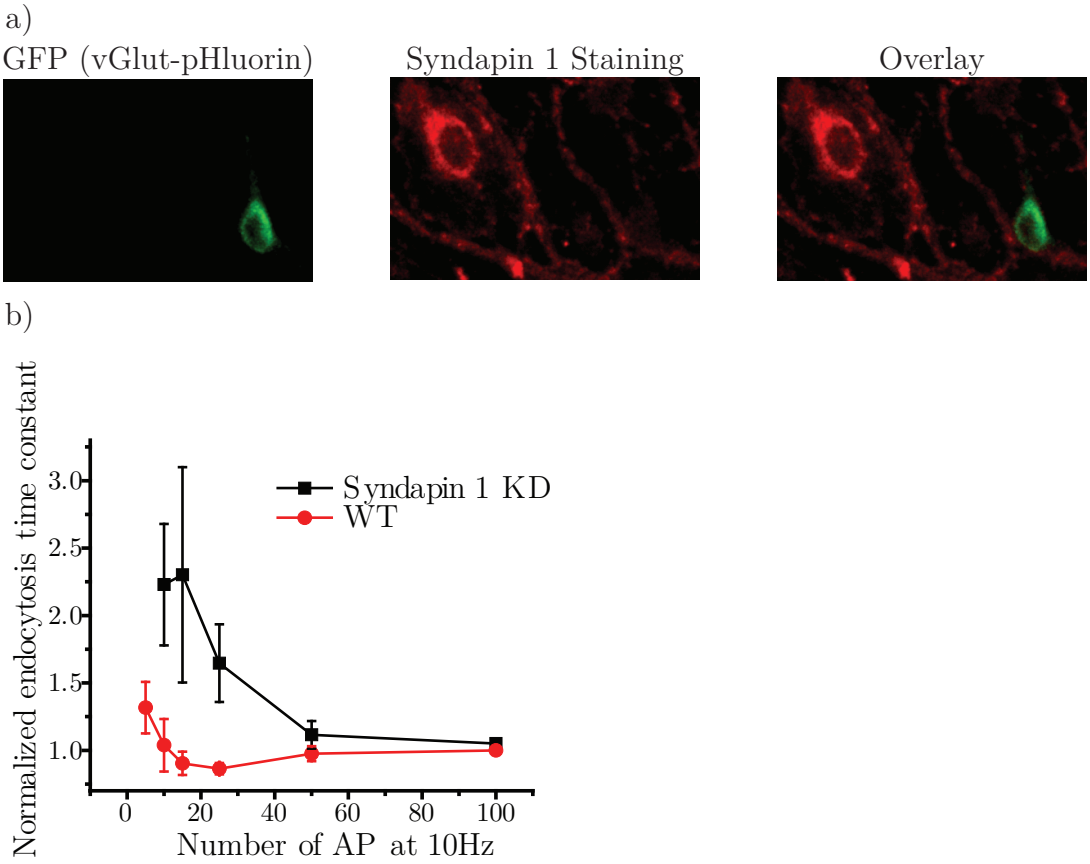

Figure 5.8: a) example of syndapin 1 KD staining, anti-GFP identifies transfected cell, anti-Syndapin 1 staining is compared in the transfected versus untransfected cells. On average $79.4 \pm 0.1\%$ KD (n=9). b) WT and Syndapin 1 KD curves plotting the stimulus dependence of endocytosis, normalized to WT 100AP 10Hz time constant. The syndapin 1 KD shifts the Ca^{2+} dependence curve rightwards, at 25AP significant difference t-test $p < 0.04$.

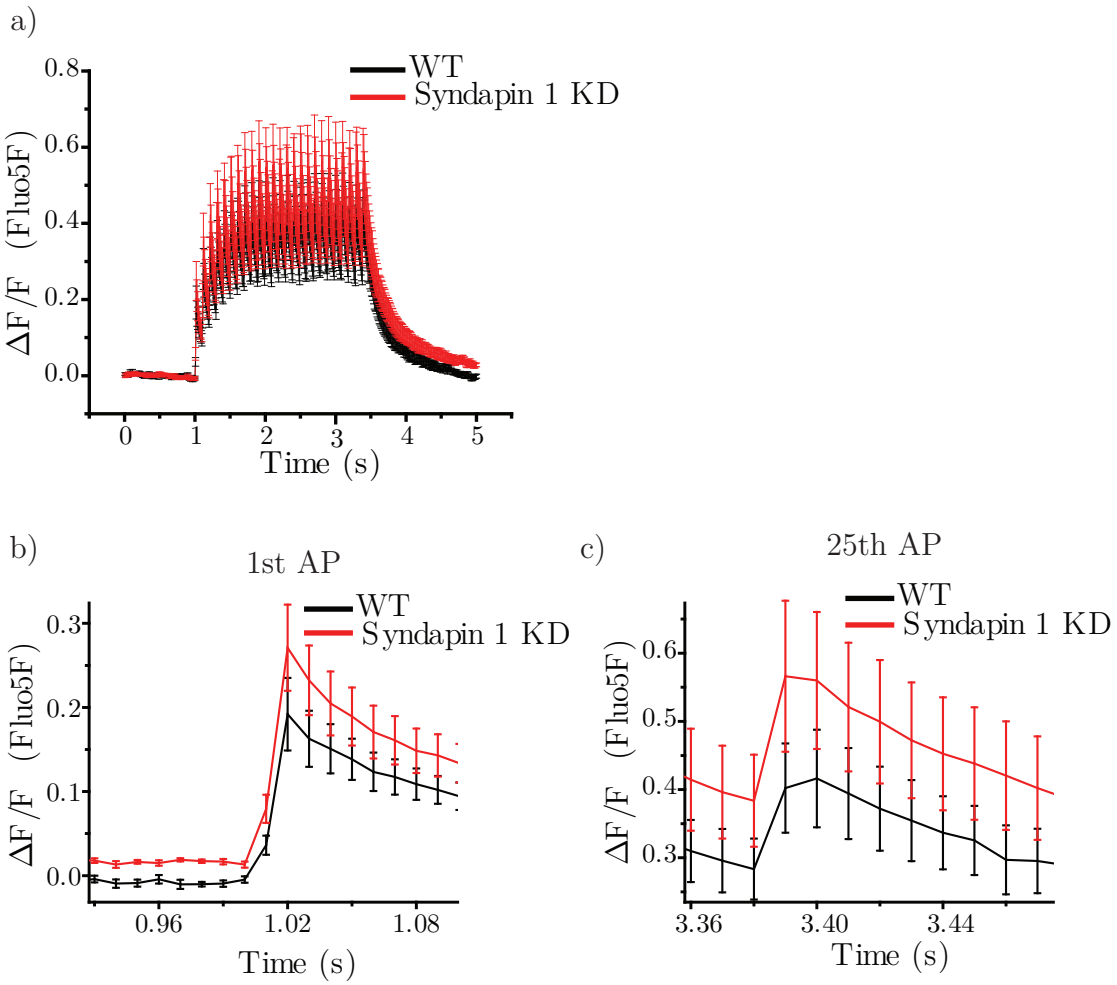

Figure 5.9: a) Imaging of Ca^{2+} influx under WT, in response to 25AP 10Hz stimulation using Fluo5F-AM. n=7 Syndapin 1 KD, n=8 cells WT b) the 1st AP from (a) no significant difference t-test p=0.37 c) the 25th AP from (a) no significant difference t-test p=0.41.

II and III present it might not be able to completely phenocopy the dynamin 1 phosphomimetic mutant. However the shift in the acceleration phase implies that a much larger stimulus is required accelerate endocytosis to the baseline time constant, consistent with dynamins desphosphorylation being required for acceleration. Finally as it is possible that the absence of syndapin I was impacting either Ca^{2+} entry or handling we carried out measurements of Ca^{2+} influx using the Ca^{2+} dye Fluo5F-AM. These experiments showed however that there was no significant difference in Ca^{2+} level after the first or last action potential, and therefore rule out a trivial explanation for the shift in Ca^{2+} sensitivity (Fig 5.9).

5.4 Discussion

Using our high-sensitivity endocytosis assays for individual neurons we revealed the presence of two phases of stimulus-dependence of synaptic vesicle endocytosis that appear to heightened at physiological temperature with brief bursts of stimuli. These data help explain previously contradictory results which showed a mix of Ca^{2+} acceleration and slowing, but failed to define what regimes were governed by these. The Ca^{2+} dependent slowing phase was more prominent at lower temperatures and agrees well with previous findings that show Ca^{2+} inhibition of endocytosis [8,94,104]. Part of this slowing phase was also missed in some studies that found no stimulus dependence [8, 30, 112]; however, this could primarily be explained by the increased sensitivity of the assay. The Ca^{2+} sensor for this mechanism is not known and remains an open question. The acceleration effects of Ca^{2+} shown before at room temperature used extremely low Ca^{2+} levels to evoke it [84,108]. We demonstrated the importance and relevance of examining such dynamics at more physiological conditions, which could reveal effects otherwise masked.

We have shown a role for dynamins phosphorylation state in synaptic vesicle

endocytosis; a question which has lingered in the field for a long time. Dynamins phosphorylation state was critical to its discovery [29, 57, 77] and has been shown to play a role in the binding of syndapin 1 to dynamin 1. The phosphorylation state also sets dynamin 1 and 3 apart from dynamin 2, the non-neuronal isoform. Some previous attempts to explore the importance of dynamins phosphorylation in synaptic vesicle endocytosis relied on inhibitors of calcineurin. However, recent work has shown that inhibiting calcineurin affects calcium influx as well as the size of the recycling pool [46, 47], thereby complicating the interpretation of those experiments. Previous measurements of dynamins dephosphorylation reported that very large stimuli were required to dephosphorylate the majority of dynamin present in synaptosomes [17, 29]. Our data however indicate that small stimuli (25AP 10Hz) are required to reach the maximum acceleration suggesting that very little dynamin is likely dephosphorylated for these conditions. Although our data show that loss of dynamins phosphorylation-dependent binding partner, syndapin 1, partially mimics having dynamin in a phosphomimetic state, it is unclear if is syndapin 1 which serves to accelerate endocytosis by being recruited by dephospho-dynamin or of dephosphodynamin serves to accelerate endocytosis by being recruited by syndapin 1. The stimulation-endocytosis curve dependence we observed indicates that there is a stimulus for which the endocytic time constant is optimized. From the point of view of endocytosis it appears that neurons are tuned to favor recovery from bursts of action potential stimulation. This suggests that cells might potentially tune their endocytic profile to be optimized for their individual firing patterns. One implication of this that is unclear however, is whether endocytosis rates are ever limiting under physiological firing regimes. Knockouts of endocytic proteins, such as amphiphysin or dynamin 1, that yielded only relatively subtle endocytic phenotypes still resulted in cognitive defects or mice that did not thrive [22, 25] suggesting that operationally endocytosis may become rate limiting in certain neuronal circuits. Dynamin is rephosphorylated

by cyclindependentkinase 5 (CDK5), the balance of activity with calcineurin also controls the size of the recycling pool. The balance of this activity has been shown to vary bouton to bouton leading to larger or smaller recycling pool sizes [46]. This suggests that the dephosphin regulation of endocytosis could be tuned at an individual synapse level. It has been suggested for example that endocytosis might play a role in clearing release sites. Thus instead of the vesicle pool being limiting for exocytosis, the clearance of release sites could limit exocytosis [66]. The mechanism of the clearance is not known but endocytic proteins have been shown to be involved [44]. This suggests that potentially the endocytic rates are far more critical for overall function than would be otherwise appreciated.

Bibliography

[1] Fredrik Andersson, Joel Jakobsson, Peter Löw, Oleg Shupliakov, and Lennart Brodin. Perturbation of syndapin/PACSIN impairs synaptic vesicle recycling evoked by intense stimulation. *The Journal of neuroscience : the official journal of the Society for Neuroscience*, 28(15):3925–3933, April 2008.

[2] Victor Anggono and Phillip J Robinson. Syndapin I and endophilin I bind overlapping proline-rich regions of dynamin I: role in synaptic vesicle endocytosis. *Journal of neurochemistry*, 102(3):931–943, August 2007.

[3] Victor Anggono, Karen J Smillie, Mark E Graham, Valentina A Valova, Michael A Cousin, and Phillip J Robinson. Syndapin I is the phosphorylation-regulated dynamin I partner in synaptic vesicle endocytosis. *Nature neuroscience*, 9(6):752–760, June 2006.

[4] A M Aravanis, J L Pyle, N C Harata, and R W Tsien. Imaging single synaptic vesicles undergoing repeated fusion events: kissing, running, and kissing again. *Neuropharmacology*, 45(6):797–813, November 2003.

[5] Pablo Ariel and Timothy A Ryan. Optical mapping of release properties in synapses. *Frontiers in neural circuits*, 4, 2010.

[6] Ryan Ariel. *Exploring Synaptic Vesicle Exocytosis*. PhD thesis, Rockefeller University, New York, October 2011.

[7] Pradeep P Atluri and Timothy A Ryan. The kinetics of synaptic vesicle reacidification at hippocampal nerve terminals. *The Journal of neuroscience : the official journal of the Society for Neuroscience*, 26(8):2313–2320, February 2006.

[8] J Balaji, Moritz Armbruster, and Timothy A Ryan. Calcium control of endocytic capacity at a CNS synapse. *The Journal of neuroscience : the official journal of the Society for Neuroscience*, 28(26):6742–6749, June 2008.

[9] J Balaji and T A Ryan. Single-vesicle imaging reveals that synaptic vesicle exocytosis and endocytosis are coupled by a single stochastic mode. *Proceedings of the National Academy of Sciences of the United States of America*, 104(51):20576–20581, December 2007.

[10] Pavel V Bashkirov, Sergey A Akimov, Alexey I Evseev, Sandra L Schmid, Joshua Zimmerberg, and Vadim A Frolov. GTPase cycle of dynamin is coupled to membrane squeeze and release, leading to spontaneous fission. *Cell*, 135(7):1276–1286, December 2008.

[11] D Beutner, T Voets, E Neher, and T Moser. Calcium dependence of exocytosis and endocytosis at the cochlear inner hair cell afferent synapse. *Neuron*, 29(3):681–690, March 2001.

[12] Tiago Branco, Kevin Staras, Kevin J Darcy, and Yukiko Goda. Local dendritic activity sets release probability at hippocampal synapses. *Neuron*, 59(3):475–485, August 2008.

[13] H Cao and F Garcia. Differential Distribution of Dynamin Isoforms in Mammalian Cells. *Molecular biology of the cell*, 1998.

[14] William A Catterall and Alexandra P Few. Calcium channel regulation and presynaptic plasticity. *Neuron*, 59(6):882–901, September 2008.

[15] M S Chen, R A Obar, C C Schroeder, T W Austin, C A Poodry, S C Wadsworth, and R B Vallee. Multiple forms of dynamin are encoded by shibire, a Drosophila gene involved in endocytosis. *Nature*, 351(6327):583–586, June 1991.

[16] E L Clayton and M A Cousin. Differential labelling of bulk endocytosis in nerve terminals by FM dyes. *Neurochemistry international*, 53(3-4):51–55, September 2008.

[17] Emma L Clayton, Victor Anggono, Karen J Smillie, Ngoc Chau, Phillip J Robinson, and Michael A Cousin. The phospho-dependent dynamin-syndapin interaction triggers activity-dependent bulk endocytosis of synaptic vesicles. *The Journal of neuroscience : the official journal of the Society for Neuroscience*, 29(24):7706–7717, June 2009.

[18] Emma L Clayton, Gareth J O Evans, and Michael A Cousin. Activity-dependent control of bulk endocytosis by protein dephosphorylation in central nerve terminals. *The Journal of physiology*, 585(Pt 3):687–691, December 2007.

[19] Emma L Clayton, Gareth J O Evans, and Michael A Cousin. Bulk synaptic vesicle endocytosis is rapidly triggered during strong stimulation. *The Journal of neuroscience : the official journal of the Society for Neuroscience*, 28(26):6627–6632, June 2008.

[20] Emma L Clayton, Nancy Sue, Karen J Smillie, Timothy O'Leary, Nicolai Bache, Giselle Cheung, Adam R Cole, David J Wyllie, Calum Sutherland, Phillip J Robinson, and Michael A Cousin. Dynamin I phosphorylation by GSK3 controls activity-dependent bulk endocytosis of synaptic vesicles. *Nature neuroscience*, 13(7):845–851, July 2010.

[21] M A Cousin and P J Robinson. The dephosphins: dephosphorylation by calcineurin triggers synaptic vesicle endocytosis. *Trends in neurosciences*, 24(11):659–665, November 2001.

[22] Gilbert Di Paolo, Sethuraman Sankaranarayanan, Markus R Wenk, Laurie Daniell, Ezio Perucco, Barbara J Caldarone, Richard Flavell, Marina R Picciotto, Timothy A Ryan, Ottavio Cremona, and Pietro De Camilli. Decreased synaptic vesicle recycling efficiency and cognitive deficits in amphiphysin 1 knockout mice. *Neuron*, 33(5):789–804, February 2002.

[23] Robert C Elston and William Davis Johnson. *Basic biostatistics for geneticists and epidemiologists*. a practical approach. Wiley, December 2008.

[24] Emma Evergren, Melissa Marcucci, Nikolay Tomilin, Peter Löw, Vladimir Slepnev, Fredrik Andersson, Helge Gad, Lennart Brodin, Pietro De Camilli, and Oleg Shupliakov. Amphiphysin is a component of clathrin coats formed during synaptic vesicle recycling at the lamprey giant synapse. *Traffic (Copenhagen, Denmark)*, 5(7):514–528, July 2004.

[25] Shawn M Ferguson, Gabor Brasnjo, Mitsuko Hayashi, Markus Wölfel, Chiara Collesi, Silvia Giovedi, Andrea Raimondi, Liang-Wei Gong, Pablo Ariel, Summer Paradise, Eileen O'Toole, Richard Flavell, Ottavio Cremona, Gero Miesenböck, Timothy A Ryan, and Pietro De Camilli. A selective activity-dependent requirement for dynamin 1 in synaptic vesicle endocytosis. *Science (New York, N.Y.)*, 316(5824):570–574, April 2007.

[26] Tomas Fernandez-Alfonso, Ricky Kwan, and Timothy A Ryan. Synaptic vesicles interchange their membrane proteins with a large surface reservoir during recycling. *Neuron*, 51(2):179–186, July 2006.

[27] Tomas Fernandez-Alfonso and Timothy A Ryan. The kinetics of synaptic vesicle pool depletion at CNS synaptic terminals. *Neuron*, 41(6):943–953, March 2004.

[28] H Gad, N Ringstad, P Löw, O Kjaerulff, J Gustafsson, M Wenk, G Di Paolo, Y Nemoto, J Crun, M H Ellisman, P De Camilli, O Shupliakov, and L Brodin. Fission and uncoating of synaptic clathrin-coated vesicles are perturbed by disruption of interactions with the SH3 domain of endophilin. *Neuron*, 27(2):301–312, August 2000.

[29] Mark E Graham, Victor Anggono, Nicolai Bache, Martin R Larsen, George E Craft, and Phillip J Robinson. The in vivo phosphorylation sites of rat brain dynamin I. *The Journal of biological chemistry*, 282(20):14695–14707, May 2007.

[30] Björn Granseth, Benjamin Odermatt, Stephen J Royle, and Leon Lagnado. Clathrin-mediated endocytosis is the dominant mechanism of vesicle retrieval at hippocampal synapses. *Neuron*, 51(6):773–786, September 2006.

[31] Björn Granseth, Benjamin Odermatt, Stephen J Royle, and Leon Lagnado. Clathrin-mediated endocytosis: the physiological mechanism of vesicle retrieval at hippocampal synapses. *The Journal of physiology*, 585(Pt 3):681–686, December 2007.

[32] Yunyun Han, Pascal S Kaeser, Thomas C Südhof, and Ralf Schneggenburger. RIM determines Ca+ channel density and vesicle docking at the presynaptic active zone. *Neuron*, 69(2):304–316, January 2011.

[33] Callista B Harper, Sally Martin, Tam H Nguyen, Shari J Daniels, Nickolas A Lavidis, Michel R Popoff, Gordana Hadzic, Anna Mariana, Ngoc Chau, Adam McCluskey, Phillip J Robinson, and Frederic A Meunier. Dynamin inhibition blocks botulinum neurotoxin type A endocytosis in neurons and delays

botulism. *The Journal of biological chemistry*, 286(41):35966–35976, October 2011.

[34] K M Harris and P Sultan. Variation in the number, location and size of synaptic vesicles provides an anatomical basis for the nonuniform probability of release at hippocampal CA1 synapses. *Neuropharmacology*, 34(11):1387–1395, November 1995.

[35] J E Heuser and T S Reese. Evidence for recycling of synaptic vesicle membrane during transmitter release at the frog neuromuscular junction. *The Journal of cell biology*, 57(2):315–344, May 1973.

[36] J E Hinshaw. Dynamin and its role in membrane fission. *Annual review of cell and developmental biology*, 16:483–519, 2000.

[37] A Hlavova, D I Abramson, B L Rickert, and J F Talso. Temperature effects on duration and amplitude of distal median nerve action potential. *Journal of applied physiology*, 28(6):808–812, June 1970.

[38] Matthew Holt, Anne Cooke, Minnie M Wu, and Leon Lagnado. Bulk membrane retrieval in the synaptic terminal of retinal bipolar cells. *The Journal of neuroscience : the official journal of the Society for Neuroscience*, 23(4):1329–1339, February 2003.

[39] Peer Hoopmann, Annedore Punge, Sina V Barysch, Volker Westphal, Johanna Bückers, Felipe Opazo, Ioanna Bethani, Marcel A Lauterbach, Stefan W Hell, and Silvio O Rizzoli. Endosomal sorting of readily releasable synaptic vesicles. *Proceedings of the National Academy of Sciences of the United States of America*, 107(44):19055–19060, November 2010.

[40] Nobutake Hosoi, Matthew Holt, and Takeshi Sakaba. Calcium dependence of exo- and endocytotic coupling at a glutamatergic synapse. *Neuron*, 63(2):216–229, July 2009.

[41] Yunfeng Hua, Raunak Sinha, Cora S Thiel, Roman Schmidt, Jana Hüve, Henrik Martens, Stefan W Hell, Alexander Egner, and Jürgen Klingauf. A readily retrievable pool of synaptic vesicles. *Nature neuroscience*, 14(7):833–839, July 2011.

[42] Zhaolin Hua, Sergio Leal-Ortiz, Sarah M Foss, Clarissa L Waites, Craig C Garner, Susan M Voglmaier, and Robert H Edwards. v-SNARE composition distinguishes synaptic vesicle pools. *Neuron*, 71(3):474–487, August 2011.

[43] Joel Jakobsson, Helge Gad, Fredrik Andersson, Peter Löw, Oleg Shupliakov, and Lennart Brodin. Role of epsin 1 in synaptic vesicle endocytosis. *Proceedings of the National Academy of Sciences of the United States of America*, 105(17):6445–6450, April 2008.

[44] Fumiko Kawasaki, Janani Iyer, Lisa L Posey, Chichun E Sun, Samantha E Mammen, Huaru Yan, and Richard W Ordway. The DISABLED protein functions in CLATHRIN-mediated synaptic vesicle endocytosis and exoendocytic coupling at the active zone. *Proceedings of the National Academy of Sciences of the United States of America*, 108(25):E222–9, June 2011.

[45] Sung Hyun Kim and Timothy A Ryan. Synaptic vesicle recycling at CNS snapses without AP-2. *The Journal of neuroscience : the official journal of the Society for Neuroscience*, 29(12):3865–3874, March 2009.

[46] Sung Hyun Kim and Timothy A Ryan. CDK5 serves as a major control point in neurotransmitter release. *Neuron*, 67(5):797–809, September 2010.

[47] Sung Hyun Kim and Timothy A Ryan. Control of presynaptic N-type calcium channel function by calcineurin Aa and CDK5. *Neuron (submitted)*, February 2012.

[48] D E Klein, A Lee, D W Frank, M S Marks, and M A Lemmon. The pleckstrin homology domains of dynamin isoforms require oligomerization for high affinity phosphoinositide binding. *The Journal of biological chemistry*, 273(42):27725–27733, October 1998.

[49] Vitaly A Klyachko and Meyer B Jackson. Capacitance steps and fusion pores of small and large-dense-core vesicles in nerve terminals. *Nature*, 418(6893):89–92, July 2002.

[50] Dennis Koch, Isabella Spiwoks-Becker, Victor Sabanov, Anne Sinning, Tamar Dugladze, Anne Stellmacher, Rashmi Ahuja, Julia Grimm, Susann Schüler, Anke Müller, Frank Angenstein, Tariq Ahmed, Alexander Diesler, Markus Moser, Susanne Tom Dieck, Rainer Spessert, Tobias Maria Boeckers, Reinhard Fässler, Christian Andreas Hübner, Detlef Balschun, Tengis Gloveli, Michael Manfred Kessels, and Britta Qualmann. Proper synaptic vesicle formation and neuronal network activity critically rely on syndapin I. *The EMBO journal*, 30(24):4955–4969, December 2011.

[51] J H Koenig and K Ikeda. Evidence for a presynaptic blockage of transmission in a temperature-sensitive mutant of Drosophila. *Journal of neurobiology*, 14(6):411–419, November 1983.

[52] J H Koenig, K Saito, and K Ikeda. Reversible control of synaptic transmission in a single gene mutant of Drosophila melanogaster. *The Journal of cell biology*, 96(6):1517–1522, June 1983.

[53] H Kuromi, M Yoshihara, and Y Kidokoro. An inhibitory role of calcineurin in endocytosis of synaptic vesicles at nerve terminals of Drosophila larvae. *Neuroscience research*, 27(2):101–113, February 1997.

[54] M M Lai, J J Hong, A M Ruggiero, P E Burnett, V I Slepnev, P De Camilli, and S H Snyder. The calcineurin-dynamin 1 complex as a calcium sensor for synaptic vesicle endocytosis. *The Journal of biological chemistry*, 274(37):25963–25966, September 1999.

[55] M M Lai, H R Luo, P E Burnett, J J Hong, and S H Snyder. The calcineurin-binding protein cain is a negative regulator of synaptic vesicle endocytosis. *The Journal of biological chemistry*, 275(44):34017–34020, November 2000.

[56] Martin R Larsen, Mark E Graham, Phillip J Robinson, and Peter Roepstorff. Improved detection of hydrophilic phosphopeptides using graphite powder microcolumns and mass spectrometry: evidence for in vivo doubly phosphorylated dynamin I and dynamin III. *Molecular & cellular proteomics : MCP*, 3(5):456–465, May 2004.

[57] J P Liu, K A Powell, T C Südhof, and P J Robinson. Dynamin I is a Ca(2+)-sensitive phospholipid-binding protein with very high affinity for protein kinase C. *The Journal of biological chemistry*, 269(33):21043–21050, August 1994.

[58] J P Liu, A T Sim, and P J Robinson. Calcineurin inhibition of dynamin I GTPase activity coupled to nerve terminal depolarization. *Science (New York, N.Y.)*, 265(5174):970–973, August 1994.

[59] Meera Mani, Sang Yoon Lee, Louise Lucast, Ottavio Cremona, Gilbert Di Paolo, Pietro De Camilli, and Timothy A Ryan. The dual phosphatase activity of synaptojanin1 is required for both efficient synaptic vesicle endocytosis and reavailability at nerve terminals. *Neuron*, 56(6):1004–1018, December 2007.

[60] Meera Mani and Timothy A Ryan. Live imaging of synaptic vesicle release and retrieval in dopaminergic neurons. *Frontiers in neural circuits*, 3:3, 2009.

[61] Kristina D Micheva and Stephen J Smith. Strong effects of subphysiological temperature on the function and plasticity of mammalian presynaptic terminals. *The Journal of neuroscience : the official journal of the Society for Neuroscience*, 25(33):7481–7488, August 2005.

[62] T M Miller and J E Heuser. Endocytosis of synaptic vesicle membrane at the frog neuromuscular junction. *The Journal of cell biology*, 98(2):685–698, February 1984.

[63] Ira Milosevic, Silvia Giovedi, Xuelin Lou, Andrea Raimondi, Chiara Collesi, Hongying Shen, Summer Paradise, Eileen O'Toole, Shawn Ferguson, Ottavio Cremona, and Pietro De Camilli. Recruitment of endophilin to clathrin-coated pit necks is required for efficient vesicle uncoating after fission. *Neuron*, 72(4):587–601, November 2011.

[64] A B Muhlberg, D E Warnock, and S L Schmid. Domain structure and intramolecular regulation of dynamin GTPase. *The EMBO journal*, 16(22):6676–6683, November 1997.

[65] V N Murthy, T Schikorski, C F Stevens, and Y Zhu. Inactivity produces increases in neurotransmitter release and synapse size. *Neuron*, 32(4):673–682, November 2001.

[66] Erwin Neher. What is Rate-Limiting during Sustained Synaptic Activity: Vesicle Supply or the Availability of Release Sites. *Frontiers in synaptic neuroscience*, 2:144, 2010.

[67] G Neves and L Lagnado. The kinetics of exocytosis and endocytosis in the synaptic terminal of goldfish retinal bipolar cells. *The Journal of physiology*, 515 (Pt 1):181–202, February 1999.

[68] A Jamila Newton, Tom Kirchhausen, and Venkatesh N Murthy. Inhibition of dynamin completely blocks compensatory synaptic vesicle endocytosis. *Proceedings of the National Academy of Sciences of the United States of America*, 103(47):17955–17960, November 2006.

[69] Arndt Pechstein and Oleg Shupliakov. Taking a back seat: synaptic vesicle clustering in presynaptic terminals. *Frontiers in synaptic neuroscience*, 2:143, 2010.

[70] Kira E Poskanzer, Kurt W Marek, Sean T Sweeney, and Graeme W Davis. Synaptotagmin I is necessary for compensatory synaptic vesicle endocytosis in vivo. *Nature*, 426(6966):559–563, December 2003.

[71] J L Pyle, E T Kavalali, E S Piedras-Rentería, and R W Tsien. Rapid reuse of readily releasable pool vesicles at hippocampal synapses. *Neuron*, 28(1):221–231, October 2000.

[72] Andrea Raimondi, Shawn M Ferguson, Xuelin Lou, Moritz Armbruster, Summer Paradise, Silvia Giovedi, Mirko Messa, Nao Kono, Junko Takasaki, Valentina Cappello, Eileen O'Toole, Timothy A Ryan, and Pietro De Camilli. Overlapping role of dynamin isoforms in synaptic vesicle endocytosis. *Neuron*, 70(6):1100–1114, June 2011.

[73] Rajesh Ramachandran, Mark Surka, Joshua S Chappie, Douglas M Fowler, Ted R Foss, Byeong Doo Song, and Sandra L Schmid. The dynamin middle domain is critical for tetramerization and higher-order self-assembly. *The EMBO journal*, 26(2):559–566, January 2007.

[74] Robert Renden and Henrique von Gersdorff. Synaptic vesicle endocytosis at a CNS nerve terminal: faster kinetics at physiological temperatures and increased endocytotic capacity during maturation. *Journal of neurophysiology*, 98(6):3349–3359, December 2007.

[75] D A Richards, C Guatimosim, and W J Betz. Two endocytic recycling routes selectively fill two vesicle pools in frog motor nerve terminals. *Neuron*, 27(3):551–559, September 2000.

[76] Silvio O Rizzoli, Ioanna Bethani, Daniel Zwilling, Dirk Wenzel, Tabrez J Siddiqui, Dorothea Brandhorst, and Reinhard Jahn. Evidence for early endosome-like fusion of recently endocytosed synaptic vesicles. *Traffic (Copenhagen, Denmark)*, 7(9):1163–1176, September 2006.

[77] P J Robinson and P R Dunkley. Depolarization-dependent protein phosphorylation in rat cortical synaptosomes: the effects of calcium, strontium and barium. *Neuroscience letters*, 43(1):85–90, December 1983.

[78] Aurélien Roux, Katherine Uyhazi, Adam Frost, and Pietro De Camilli. GTP-dependent twisting of dynamin implicates constriction and tension in membrane fission. *Nature*, 441(7092):528–531, May 2006.

[79] Guy A Rutter and Takashi Tsuboi. Kiss and run exocytosis of dense core secretory vesicles. *Neuroreport*, 15(1):79–81, January 2004.

[80] T A Ryan. Inhibitors of myosin light chain kinase block synaptic vesicle pool mobilization during action potential firing. *The Journal of neuroscience : the official journal of the Society for Neuroscience*, 19(4):1317–1323, February 1999.

[81] R L Saint Marie and S D Carlson. Synaptic vesicle activity in stimulated and unstimulated photoreceptor axons in the housefly. A freeze-fracture study. *Journal of neurocytology*, 11(5):747–761, October 1982.

[82] S Sankaranarayanan, D De Angelis, J E Rothman, and T A Ryan. The use of pHluorins for optical measurements of presynaptic activity. *Biophysical journal*, 79(4):2199–2208, October 2000.

[83] S Sankaranarayanan and T A Ryan. Real-time measurements of vesicle-SNARE recycling in synapses of the central nervous system. *Nature cell biology*, 2(4):197–204, April 2000.

[84] S Sankaranarayanan and T A Ryan. Calcium accelerates endocytosis of vSNAREs at hippocampal synapses. *Nature neuroscience*, 4(2):129–136, February 2001.

[85] T Schikorski and C F Stevens. Quantitative ultrastructural analysis of hippocampal excitatory synapses. *The Journal of neuroscience : the official journal of the Society for Neuroscience*, 17(15):5858–5867, August 1997.

[86] G M Shepherd and K M Harris. Three-dimensional structure and composition of CA3–¿CA1 axons in rat hippocampal slices: implications for presynaptic connectivity and compartmentalization. *The Journal of neuroscience : the official journal of the Society for Neuroscience*, 18(20):8300–8310, October 1998.

[87] H S Shpetner and R B Vallee. Identification of dynamin, a novel mechanochemical enzyme that mediates interactions between microtubules. *Cell*, 59(3):421–432, November 1989.

[88] O Shupliakov, P Löw, D Grabs, H Gad, H Chen, C David, K Takei, P De Camilli, and L Brodin. Synaptic vesicle endocytosis impaired by dis-

ruption of dynamin-SH3 domain interactions. *Science (New York, N.Y.)*, 276(5310):259–263, April 1997.

[89] Raunak Sinha, Saheeb Ahmed, Reinhard Jahn, and Jürgen Klingauf. Two synaptobrevin molecules are sufficient for vesicle fusion in central nervous system synapses. *Proceedings of the National Academy of Sciences of the United States of America*, 108(34):14318–14323, August 2011.

[90] Karen J Smillie and Michael A Cousin. Dynamin I phosphorylation and the control of synaptic vesicle endocytosis. *Biochemical Society symposium*, (72):87–97, 2005.

[91] Stephen M Smith, Robert Renden, and Henrique von Gersdorff. Synaptic vesicle endocytosis: fast and slow modes of membrane retrieval. *Trends in neurosciences*, 31(11):559–568, November 2008.

[92] Byeong Doo Song, Marilyn Leonard, and Sandra L Schmid. Dynamin GTPase domain mutants that differentially affect GTP binding, GTP hydrolysis, and clathrin-mediated endocytosis. *The Journal of biological chemistry*, 279(39):40431–40436, September 2004.

[93] J M Sontag, E M Fykse, Y Ushkaryov, J P Liu, P J Robinson, and T C Südhof. Differential expression and regulation of multiple dynamins. *The Journal of biological chemistry*, 269(6):4547–4554, February 1994.

[94] Jian-Yuan Sun, Xin-Sheng Wu, and Ling-Gang Wu. Single and multiple vesicle fusion induce different rates of endocytosis at a central synapse. *Nature*, 417(6888):555–559, May 2002.

[95] Tao Sun, Xin-Sheng Wu, Jianhua Xu, Benjamin D McNeil, Zhiping P Pang, Wanjun Yang, Li Bai, Syed Qadri, Jeffery D Molkentin, David T Yue, and

Ling-Gang Wu. The role of calcium/calmodulin-activated calcineurin in rapid and slow endocytosis at central synapses. *The Journal of neuroscience : the official journal of the Society for Neuroscience*, 30(35):11838–11847, September 2010.

[96] S M Sweitzer and J E Hinshaw. Dynamin undergoes a GTP-dependent conformational change causing vesiculation. *Cell*, 93(6):1021–1029, June 1998.

[97] Shigeo Takamori, Matthew Holt, Katinka Stenius, Edward A Lemke, Mads Grønborg, Dietmar Riedel, Henning Urlaub, Stephan Schenck, Britta Brügger, Philippe Ringler, Shirley A Müller, Burkhard Rammner, Frauke Gräter, Jochen S Hub, Bert L De Groot, Gottfried Mieskes, Yoshinori Moriyama, Jürgen Klingauf, Helmut Grubmüller, John Heuser, Felix Wieland, and Reinhard Jahn. Molecular anatomy of a trafficking organelle. *Cell*, 127(4):831–846, November 2006.

[98] K Takei, O Mundigl, L Daniell, and P De Camilli. The synaptic vesicle cycle: a single vesicle budding step involving clathrin and dynamin. *The Journal of cell biology*, 133(6):1237–1250, June 1996.

[99] Haibing Teng, Michael Y Lin, and Robert S Wilkinson. Macroendocytosis and endosome processing in snake motor boutons. *The Journal of physiology*, 582(Pt 1):243–262, July 2007.

[100] Hirofumi Tokuoka and Yukiko Goda. Activity-dependent coordination of presynaptic release probability and postsynaptic GluR2 abundance at single synapses. *Proceedings of the National Academy of Sciences of the United States of America*, 105(38):14656–14661, September 2008.

[101] Gina G Turrigiano. The self-tuning neuron: synaptic scaling of excitatory synapses. *Cell*, 135(3):422–435, October 2008.

[102] A M van der Bliek and E M Meyerowitz. Dynamin-like protein encoded by the Drosophila shibire gene associated with vesicular traffic. *Nature*, 351(6325):411–414, May 1991.

[103] MG Vangel. Confidence intervals for a normal coefficient of variation. *American Statistician*, 1996.

[104] H von Gersdorff and G Matthews. Inhibition of endocytosis by elevated internal calcium in a synaptic terminal. *Nature*, 370(6491):652–655, August 1994.

[105] Martin Wienisch and Jürgen Klingauf. Vesicular proteins exocytosed and subsequently retrieved by compensatory endocytosis are nonidentical. *Nature neuroscience*, 9(8):1019–1027, August 2006.

[106] Wei Wu and Ling-Gang Wu. Rapid bulk endocytosis and its kinetics of fission pore closure at a central synapse. *Proceedings of the National Academy of Sciences of the United States of America*, 104(24):10234–10239, June 2007.

[107] Wei Wu, Jianhua Xu, Xin-Sheng Wu, and Ling-Gang Wu. Activity-dependent acceleration of endocytosis at a central synapse. *The Journal of neuroscience : the official journal of the Society for Neuroscience*, 25(50):11676–11683, December 2005.

[108] Xin-Sheng Wu, Benjamin D McNeil, Jianhua Xu, Junmei Fan, Lei Xue, Ernestina Melicoff, Roberto Adachi, Li Bai, and Ling-Gang Wu. Ca(2+) and calmodulin initiate all forms of endocytosis during depolarization at a nerve terminal. *Nature neuroscience*, 12(8):1003–1010, August 2009.

[109] Jianhua Xu, Benjamin McNeil, Wei Wu, David Nees, Li Bai, and Ling-Gang Wu. GTP-independent rapid and slow endocytosis at a central synapse. *Nature neuroscience*, 11(1):45–53, January 2008.

[110] Jing Xue, Mark E Graham, Aimee E Novelle, Nancy Sue, Noah Gray, Mark A McNiven, Karen J Smillie, Michael A Cousin, and Phillip J Robinson. Calcineurin selectively docks with the dynamin Ixb splice variant to regulate activity-dependent bulk endocytosis. *The Journal of biological chemistry*, 286(35):30295–30303, September 2011.

[111] Takayuki Yamashita, Toshihide Hige, and Tomoyuki Takahashi. Vesicle endocytosis requires dynamin-dependent GTP hydrolysis at a fast CNS synapse. *Science (New York, N.Y.)*, 307(5706):124–127, January 2005.

[112] Jun Yao, Sung E Kwon, Jon D Gaffaney, F Mark Dunning, and Edwin R Chapman. Uncoupling the roles of synaptotagmin I during endo- and exocytosis of synaptic vesicles. *Nature neuroscience*, 15(2):243–249, 2011.

[113] Lijun Yao and Takeshi Sakaba. Activity-dependent modulation of endocytosis by calmodulin at a large central synapse. *Proceedings of the National Academy of Sciences of the United States of America*, 109(1):291–296, January 2012.

[114] Yang-In Yim, Tao Sun, Ling-Gang Wu, Andrea Raimondi, Pietro De Camilli, Evan Eisenberg, and Lois E Greene. Endocytosis and clathrin-uncoating defects at synapses of auxilin knockout mice. *Proceedings of the National Academy of Sciences of the United States of America*, 107(9):4412–4417, March 2010.

[115] Qi Zhang, Yu-Qing Cao, and Richard W Tsien. Quantum dots provide an optical signal specific to full collapse fusion of synaptic vesicles. *Proceedings of the National Academy of Sciences of the United States of America*, 104(45):17843–17848, November 2007.

[116] Qi Zhang, Yulong Li, and Richard W Tsien. The dynamic control of kiss-and-run and vesicular reuse probed with single nanoparticles. *Science (New York, N.Y.)*, 323(5920):1448–1453, March 2009.

[117] Zhen Zhang, Yao Wu, Zhao Wang, F Mark Dunning, Jonathan Rehfuss, Deepshika Ramanan, Edwin R Chapman, and Meyer B Jackson. Release mode of large and small dense-core vesicles specified by different synaptotagmin isoforms in PC12 cells. *Molecular biology of the cell*, 22(13):2324–2336, July 2011.

[118] Yongling Zhu, Jian Xu, and Stephen F Heinemann. Two pathways of synaptic vesicle retrieval revealed by single-vesicle imaging. *Neuron*, 61(3):397–411, February 2009.